Emergent effects of synaptic connectivity on cortical sleep slow wave amplitude, density and propagation in a large-scale thalamocortical network model of the human brain

Brianna M Marsh[1,2†], **M. Gabriela Navas-Zuloaga**[1†], **Burke Q Rosen**[2], **Yury Sokolov**[1], **Jean Erik Delanois**[1,3], **Oscar C González**[1], **Giri P. Krishnan**[1], **Eric Halgren**[2,4], **Maxim Bazhenov**[1,2]

***For correspondence:** mbazhenov@ucsd.edu (MB)

[†]These authors contributed equally to this work

[1]Department of Medicine, University of California, San Diego ; [2]Neuroscience Graduate Program, University of California, San Diego ; [3]Department of Computer Science and Engineering, University of California, San Diego ; [4]Departments of Radiology and Neuroscience, University of California, San Diego

Abstract Slow-wave sleep (SWS), characterized by slow oscillation (SO, <1Hz) of alternating active and silent states in the thalamocortical network, is a primary brain state during Non-Rapid Eye Movement (NREM) sleep. However, the understanding of how global SO emerges from micro-scale neuron dynamics and network connectivity remains unclear. We developed a multi-scale, biophysically realistic human "whole-brain" thalamocortical network model capable of transitioning between the awake state and slow-wave sleep, and we investigated the role of connectivity in the spatio-temporal dynamics of sleep SO. SO remained robust in the face of substantial changes in connection weights, delays, sparsity, and range. However, extreme changes triggered distinct alterations in network behavior. Long synaptic delays led to the loss of downstates, while a reduction of over 50% in connection density decreased both SO frequency and amplitude. Even partial removal of local connections severely disrupted wave propagation. Lastly, reductions in long-range connection strength resulted in loss of global synchronization and led to the local propagation of slow waves. These results shed light on how the spatio-temporal properties of SO emerge from local and global cortical connectivity and provide a framework for further exploring mechanism and functions of SWS in health and diseases.

Introduction

Internal states of the brain rapidly and profoundly influence sensation, cognition, emotion, and action (***Lee and Dan, 2012***; ***Pfaff et al., 2008***; ***Steriade and McCarley, 2013***). Dramatic change of internal brain state occurs at the transition between wakefulness and sleep (***Campbell and Tobler, 1984***; ***Leung and Mourrain, 2018***; ***Steriade and McCarley, 2013***). The main electrophysiological hallmarks of slow wave sleep (SWS) and rapid eye movement (REM) sleep are shared across mammals.

During the SWS virtually all cortical neurons oscillate between an active Up and a silent Down state, the activity called slow oscillation (SO, <1Hz) (***Steriade et al., 1993a***,b). Alterations of these sleep dynamics have significant consequences for brain function and are at the core of many neuropsychiatric disorders (***Winkelman and Lecea, 2020***).

The SO repeatedly reset the thalamocortical network during the Down phase and temporally group sleep spindles, which are associated with LTP-like processes and learning, during the Up phase (***Mölle et al., 2009***; ***Rosanova and Ulrich, 2005***). These observations led to the hypothesis that SO provide a global temporal frame within the cortex and between brain regions (e.g., hippocampus, thalamus, striatum) for offline memory processing and reactivation via the strengthening of neuronal circuits (***Isomura et al., 2006***; ***Ji and Wilson, 2007***; ***Pfaff et al., 2008***; ***Rasch et al., 2007***; ***Wierzynski et al., 2009***).

Resilience to thalamic lesions and existence in cortical slices suggest the cortical origin of sleep SO (***Steriade, 2001***; ***Sanchez-Vives and McCormick, 2000***). Intracellular recordings from isolated cortical slabs revealed contribution of synaptic miniature EPSPs in intracortical synapses in Up state generation (***Timofeev et al., 2000a***; ***Bazhenov et al., 2002***). It has been shown that SOs are highly synchronous within (at least) 7mm patches in the cortex, with sharp onsets (***Destexhe et al., 1999***). Slow waves have further been observed as both Type I (global slow waves, early stages of sleep) and Type II (local slow waves, later stages of sleep) (***Siclari et al., 2014***; ***Bernardi et al., 2018***). Collectively, these evidences highlight how understanding the mechanisms contributing to SO generation and their spatio-temporal dynamics is fundamental to study slow-wave sleep.

Despite the availability of large-scale recordings and intracellular observations, how macro-scale SO emerge from the interaction between micro-scale neuronal dynamics and cortical network connectivity is still poorly understood. We previously developed computer models of sleep SO (***Timofeev et al., 2000a***; ***Bazhenov et al., 2002***), including transitions between awake and sleep states (***Krishnan et al., 2016***). However, the highly detailed and computationally intensive nature of these models have prevented up-scaling to investigate slow wave dynamics at the whole-brain scale. Recently, several whole-brain models of slow-wave sleep incorporating biologically grounded connectivity from probabilistic DTI tractography and providing a good fit to human sleep recordings were proposed (***Cakan et al., 2022***; ***Goldman et al., 2023***). These models investigated the role of long-range connections in SO brain-wide propagation. However, the mean-field neural-mass representation of cortical regions in these models provides only limited insights on how local (within a few milimeters) and long-range connectivity and activity interact to affect initiation and propagation of sleep slow waves.

To bridge this gap between micro and macro-scale mechanisms, we have developed a multi-scale, whole-brain, thalamocortical network model with biologically grounded cortical connectivity that exhibits the essential activity states of wake and slow wave sleep. The model consists of 10,242 cortical columns per hemishpere, each containing spiking pyramidal (PY) and inhibitory (IN) neurons arrayed in 6 layers, and 640 thalamic cells of each of four types (thalamo-cortical (TC) and reticular (RE), belonging to either core or matrix). Thus, our model provides unparalleled structural resolution for studying brain-wide activity patterns of the thalamocortical network during slow-wave sleep. To investigate the role of connectivity in emerging SO, we systematically modified the delays, density, range, and relative strength of cortical connections, as well as distance-dependent synaptic delays, and quantified their effect on the resulting large-scale slow-wave dynamics. Our multi-scale model of the entire brain elucidates how the global structure of intracortical connections gives rise to the characteristic spatio-temporal properties of slow oscillations, incliding local sleep, and provides a novel framework for future investigation into disruptions and disorders of slow-wave sleep.

Results

Connectivity

We start with a brief overview of the model (see Methods for details) (***Figure 1***). The model includes 10,242 cortical columns positioned uniformly across the surface of one hemisphere. Each column has 6 cortical layers (L2, L3, L4, L5a, L5b and L6). Cortical neurons are modeled using computationally efficient map-based (***Komarov et al., 2018***) spiking PY and IN neurons. Intra-columnar connections follow the canonical cortical circuit (***Figure 1***A), while long-range cortical connectivity (***Figure 1***B) is based on DTI tractography between parcels determined by the Human Connectome Project (HPC) (***Rosen and Halgren, 2021***), originating and terminating in layers according to the parcel's relative hierarchical positions (***Figure 1***D-E) . Column-wise connectivity is obtained by applying the parcel-wise relation between connection length and probability to synthesized intercolumnar distances (***Figure 1***C, see Diffusion MRI Guided Connection Probability for details). The resulting connectivity (***Figure 1***G) retains the parcelwise structure form the data in ***Rosen and Halgren*** (***2021***) (***Figure 1***F) , with an approximately exponential distribution between connection frequency and length (see ***Figure 1***C). The connection delays, which are proportional to the geodesic connection lengths, follow a similar distribution. The thalamus is simulated with layers of thalamocortical (TC) and reticular thalamic (RE) neurons (***Bazhenov et al., 1998a***,b, ***2002***), and consists of the core and the matrix (***Bonjean et al., 2011***, ***2012***), which selectively project to the neurons from different cortical layers satisfying the outlined cortico-thalamo-cortical loop (***Shepherd and Yamawaki, 2021***). Following (***Krishnan et al., 2016***) the model included the effects of neuromodulators - Acetylcholine, Norepinephrine and GABA - to simulate transitions between Wake state and SWS.

In the following sections, we first discuss "baseline" awake and sleep state dynamics of the model and then we discuss effects of alternating network connectivity on SWS. Effects are primarily described in terms of 3 key metrics: *synchrony*, *spread*, and *participation*. Synchrony refers to the timing of the Up state onsets & offsets across all neurons participating in a slow wave. Spread refers to how far the slow wave travels across the cortex. Finally, participation refers to the percent of neurons that participate in the slow wave within the area of spread.

Wake State Characterization

Wake state (***Figure 2***A) was tuned to show a consistent average firing rate of individual neurons at about 12.55 Hz. The power spectral density (***Figure 2***a.5) revealed a distinct $1/f$ phenomenon, as is common for in vivo recordings from awake state (***Donoghue et al., 2020***). Single cell voltages showed irregular firing (***Figure 2***a.1), with a peak in the voltage histogram representing baseline membrane voltage around -65 mV (***Figure 2***a.4). Individual neurons were not synchronized in their firing (***Figure 2***a.3), which was reflected in the nearly flat LFP (***Figure 2***a.2). Overall, the network revealed properties representative of biological wake state brain activity.

Slow Wave Characterization

To attain a network displaying SWS-like activity from the wake state baseline, several cellular and neurochemical parameters were adjusted according to the methodology presented in (***Krishnan et al., 2016***). Namely, we increased cortical AMPA, GABA, and potassium leak currents, thalamic GABA, and TC cell leak currents, but decreased in RE cell leak currents.

The resulting baseline model of SWS (***Figure 2***B) revealed synchronized and regular slow waves in all cortical excitatory and inhibitory neurons (***Figure 2***b.1) with approximately 0.27 Hz frequency, 26 mV peak-to-trough-amplitude (***Figure 2***b.2), and single-cell bursting dynamics during the Up states (***Figure 2***b.3). The slow-waves were further highly synchronized across layers (Supplementary ***Figure S1***). In general, the network spent more time in the Down states, and the Up state onsets and offsets were well synchronized (see narrow onset and offset histograms in ***Figure 2***b.5). The latency maps in ***Figure 2***D demonstrate how waves of activity travel from a single initiation site, which varied between Up states with no detectable dependency on the previous ones, involving

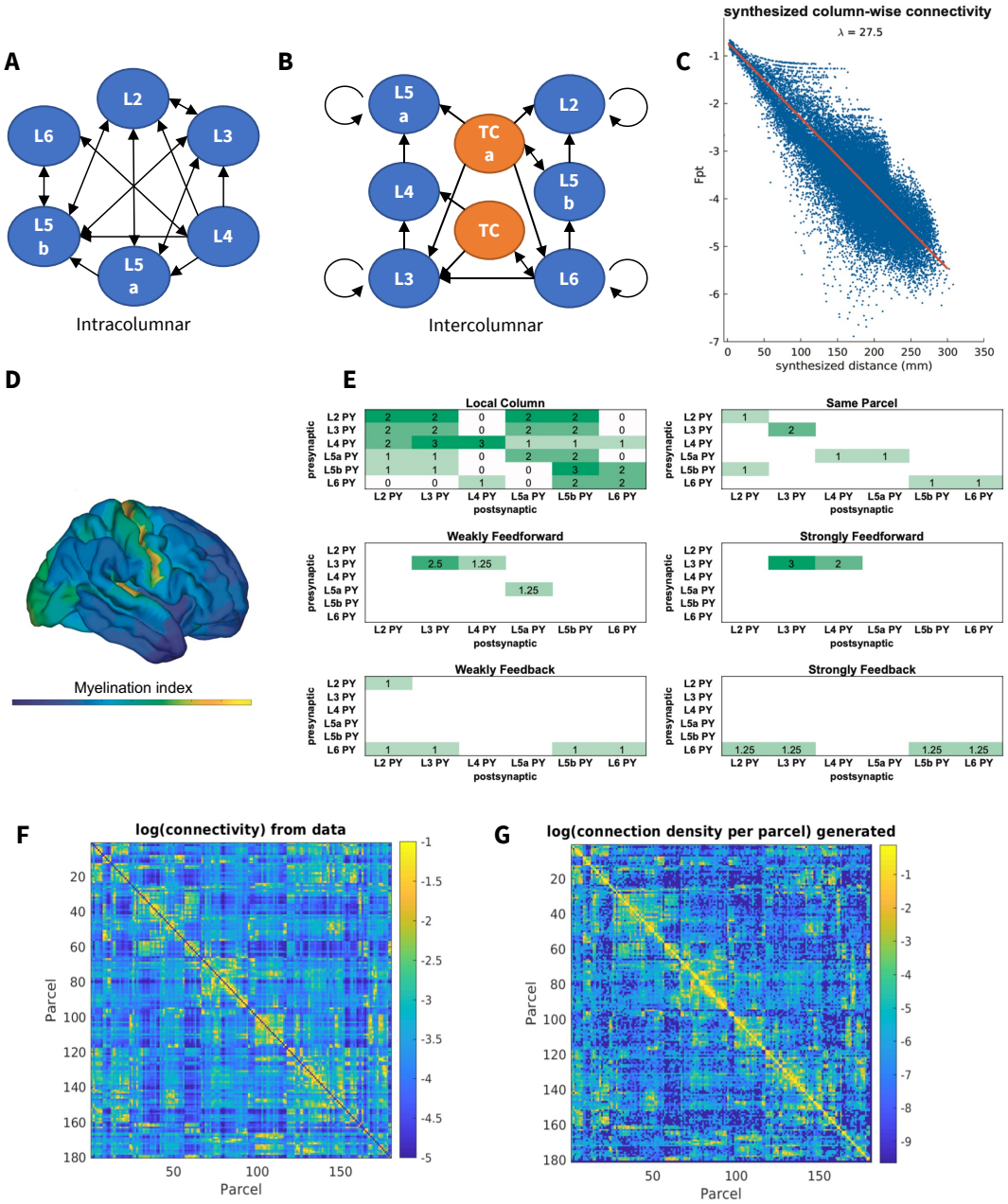

Figure 1. Model architecture. A) Connectivity between neurons in the same column follows the canonical circuit. Arrows indicate directed connections between layers. Neurons are never connected to themselves. B) Connectivity diagram between different cortical columns and thalamocortical cells in the core (TC) or matrix (TCa). C) Exponential decay of connection probability with distance between columns. Previously reported inter-parcel dMRI connectivity (***Rosen and Halgren, 2021***) shows an exponential relation with fiber distance. Columnwise connection probability is obtained by applying the dMRI exponential function to inter-column fiber distances (synthesized from their corresponding geodesic distances) and then adding the residual inter-parcel dMRI connectivity, estimated by regressing out the exponential trend (see Diffusion MRI Guided Connection Probability for details). D) Estimated myelination index (***Glasser and Essen, 2011***; ***Burt et al., 2018***) throughout the cortex. A hierarchical index inversely proportional to this myelination index is assigned to each of the 360 cortical parcels designated in the HCP-PPM1.0 atlas (***Glasser et al., 2016***). E) Excitatory corticocortical connections belong to one of 6 classes based on the hierarchical index of the pre- and post-synaptic neurons: within the same column, within the same parcel, weakly or strongly feedforward (from lower to higher hierarchical index) and weakly or strongly feedback (from higher to lower hierarchical index). Based on experimental reports on connectivity (***Markov et al., 2013***; ***Rockland, 2019***) weights are scaled according to the connection type by the factor shown in the matrices. F) Parcel-wise connectivity from ***Rosen and Halgren*** (***2021***). G) Generated model connectivity, which approximately reproduces the parcel-wise structure from data in panel F.

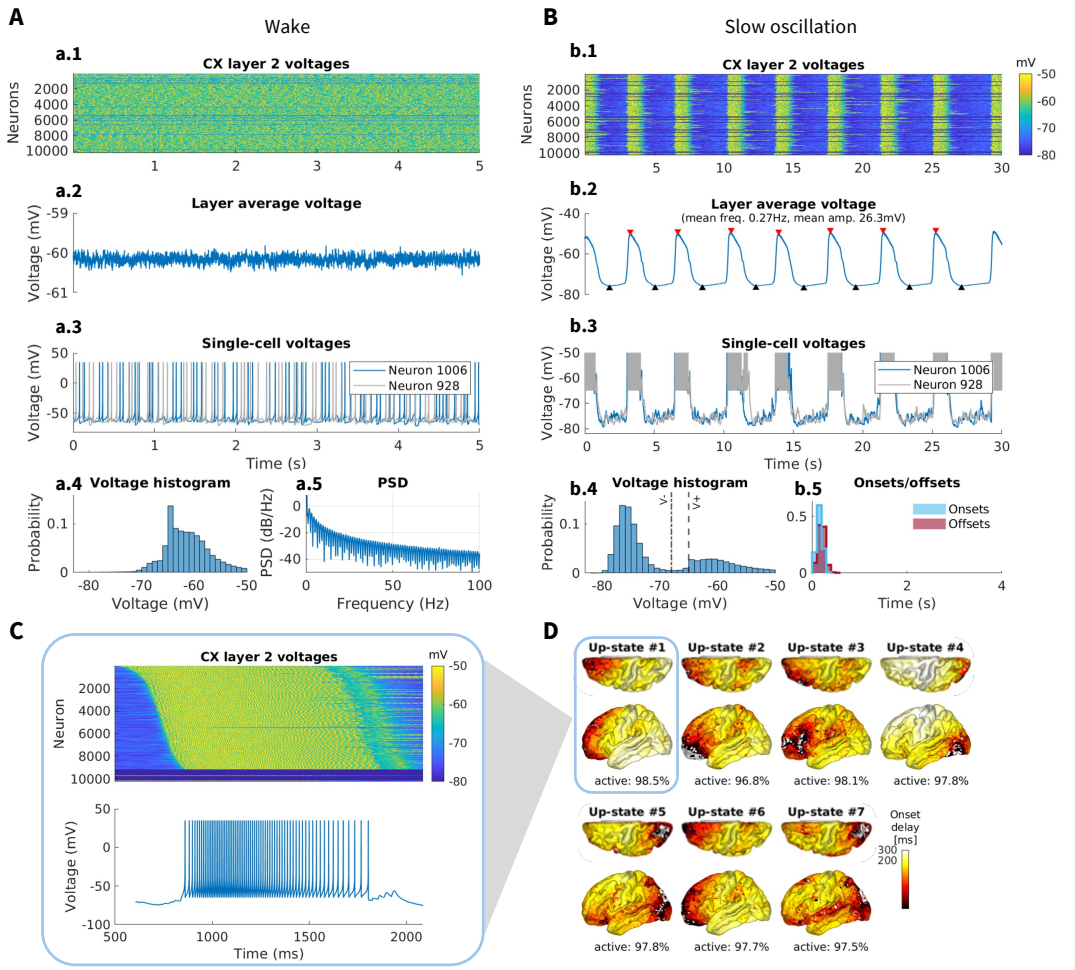

Figure 2. Baseline model activity in wake and sleep states. A) Wake state. a.1) Membrane voltages of all neurons from layer 2 over 5 seconds of simulation; a.2) Layer average voltage over time, simulating LFP; a.3) Activity of two representative neurons from layer 2, both showing irregular tonic firing; a.4) Voltage histogram of all neurons over the whole simulation time, note -65mV peak representing baseline membrane voltage; a.5) Power spectral density (PSD) of the average voltage revealed a distinct $1/f$ phenomenon typical of *in-vivo* recordings. B) Slow-wave dynamics. b.1) Membrane voltages of all neurons from layer 2 over 30 seconds of simulation, revealed synchronized bands of activity during Up states; b.2) Layer average voltage over time, with *red* and *black triangles* marking global Up and Down states; a.3) Activity of two representative neurons from layer 2, both showing synchronized activity during each upstate; a.4) Voltage histogram of all neurons over the whole simulation time, revealed the characteristic bi-modal distribution caused by Up and Down state alternations during SWS. Dashed vertical lines labeled V^- and V^+ indicate the voltage thresholds used to detect Down states and Up states, respectively; b.5) Distribution of the Up state onsets and offsets for all neurons over the whole simulation time. Narrow histograms indicate highly synchonous initiation and termination of the Up states. C) Zoom into the first Up state from panel b.1, with neurons sorted from earliest to latest onset time, and a single cell voltage from panel b.2, showing the transition from Down to Up state, steady firing during the Up state, and transition to Down state. D) Latency map, calculated as the onset delay of each neuron with respect to the earliest onset, for each Up state in panel b.2 (see Onset/offset Detection and Latency in Methods for details). The percent of active neurons during each Up state is shown below the corresponding latency map. Up-states involve nearly every modeled neuron in the cortex within 300ms from its initiation time. Moreover, a single initiation site is generally identifiable, with activity spreading progressively to farther regions of the cortex in the manner of a travelling wave.

>97% of all excitatory neurons in about 300ms. In this baseline model, slow-waves revealed both high spread and high participation. Cortical inhibitory, thalamocortical, and reticular thalamic neurons all showed similar pattern of slow oscillations (Supplementary ***Figure S2***), as previously shown in (***Bazhenov et al., 2002***).

Connection Density

In the baseline model, connections between neurons were set to match biological data (see Methods). Next, to test the effects of connection density between regions, we gradually changed the density of connections, by applying a set probability P to retain each possible connection (***Figure 3***A-B) regardless of the distance between neurons, thus keeping the connection distance distribution unchanged (***Figure 3***C). Strengths of remaining synaptic connections were scaled up to compensate for the lost connections to ensure an equivalent amount of net activation per neuron in the network (see Methods for details).

Setting the probability from 100% down to 50% (i.e., ablating a random half of all connections) had minimal effect on the slow waves, indicating the model's robustness to even significant loss of individual connections. Slow waves exhibited a similar propagation pattern with only a slightly reduced amplitude (26 mV to 24 mV) and speed (***Figure 3***D, F). The synchrony of the Up state offsets, however, was impaired; the distribution of offset timings across neuron became much wider (***Figure 3***d.5, f.5) compare to baseline model (***Figure 2***b.5). Further decreasing density below 30% caused a considerable drop in amplitude and participation (***Figure 3***f.1, f.4). In the extreme case of only 10% of connections remaining ($P = 0.1$, ***Figure 3***E), there was continued loss of synchrony in Up state offsets and onsets, slow waves became less frequent (down to 0.17 Hz), with lower amplitude (13.38 mV), and lower participation (only 70% of neurons involved per upstate) (***Figure 3***F). Nevertheless, slow waves still propagated through the all brain regions on the macro scale, showing that long range synchrony is still possible (if slightly impaired) with only very few connections in place as long as those connections are sufficiently strong and long-range connections are present. Below this level of remaining connections, slow waves were ablated and the network was largely silent.

Figure 4 shows further details into the slow-wave dynamics in the case of extreme density loss ($P = 0.1$), zooming into ten cortical regions with a 5mm radius each (***Figure 4***A). Single cells and LFPs in different regions throughout the cortex (***Figure 4***C-D) showed synchronized Up states, although number of neurons were not active during some of Up states(***Figure 4***C, E). The local heterogeneity in activation patterns induced by the extreme sparsity of connections is evident in ***Figure 4***E, which shows many silent neurons in the immediate vicinity or active cells. This generated the extremely granular participation seen in the latency maps (***Figure 4***F). Even though each Up state encompassed cells in the whole cortex (high spread), a large fraction of cells distributed through the entire cortex did not participate in slow-waves (decreased participation). Initiation was diffused with respect to the baseline simulation, to the point where a single meaningful estimate of propagation speed for each Up state could no longer be computed.

Connection Range

To determine the specific contribution of long-range connections, we varied the maximum connection radius; any connections longer than a specified distance R were ablated (***Figure 5***A). Again, the strengths of remaining connections were scaled up to compensate for reduction in the total number of connections and to keep total synaptic input per cell unchanged. In contrast to the density reduction (see ***Figure 3***C), this alternation did shift the connection distance distribution (***Figure 5***C).

The maximum connection length in baseline model was 226.1 mm, but most connections (approximately 80%) were maintained within 100 mm (***Figure 5***B). A connection radius as small as 5 mm, which includes second-order neighbors of a given neuron, resulted in only approximately 6% of connections still intact. The alterations of the maximum connection length led to significantly different activity patterns than in the network with a spatially uniform drop to the same percentage of

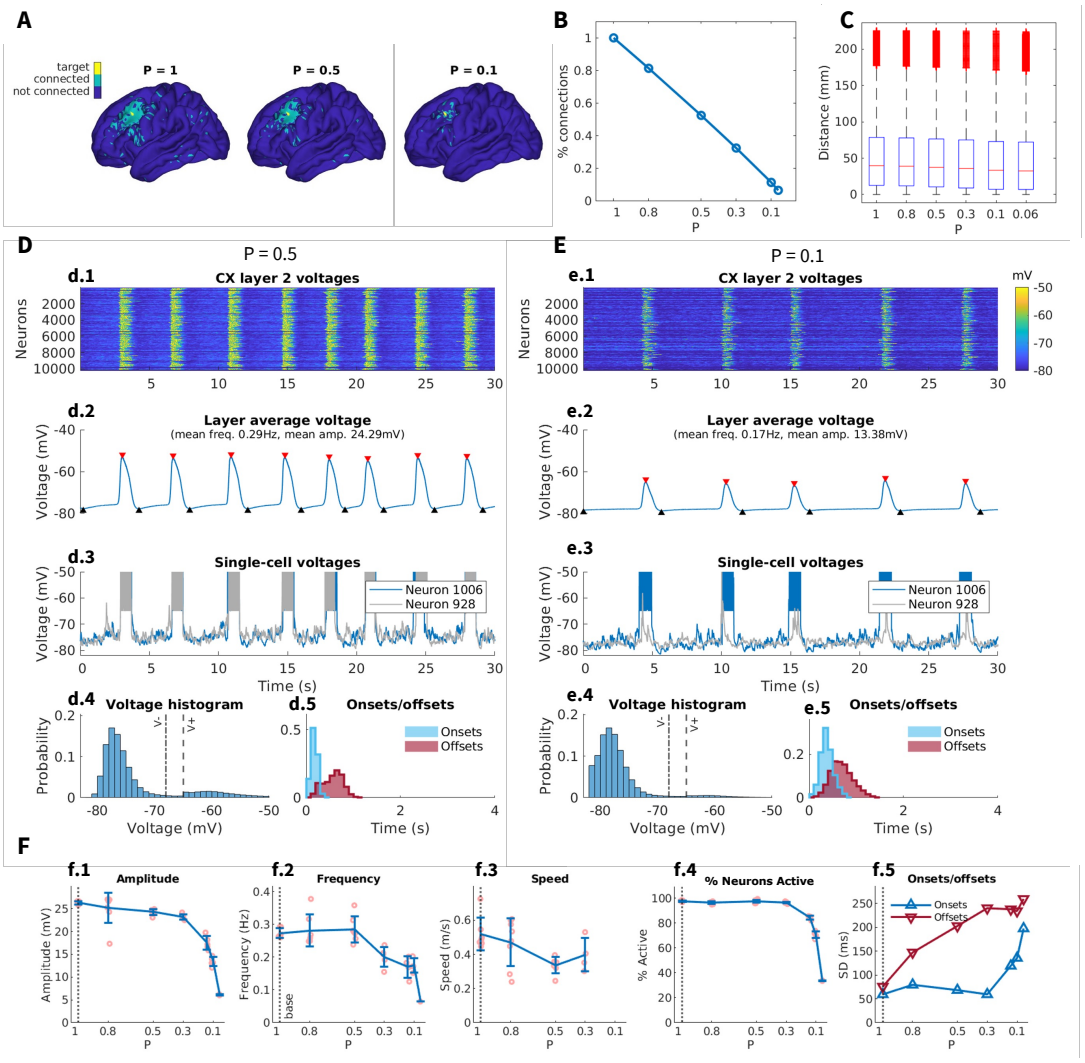

Figure 3. Effect of connection density on SO dynamics. A) Example target cortical column (*yellow*) with all columns connected to it through any layer (*green*) for different connection densities. Density is reduced by decreasing P, which denotes the probability of preserving a connection from the original dMRI-based connectivity. With $P = 1$ all connections are preserved, while for $P = 0.5$, $P = 0.3$ and $P = 0.1$ each connection is preserved with a $50\%, 30\%$ or 10% probability, respectively. B) Percent of the original number of connections retained for different values of P. C) Distribution of connection distances, or lengths, for different values of P. Red horizontal lines indicate medians, bottom and top box edges indicate the 25th and 75th percentiles, respectively, whiskers extend to the most extreme data points not considered outliers, and outliers are plotted individually using the '+' marker symbol. Note, connection density is reduced uniformly across all lengths. D-E) Individual analysis of SO dynamics for different values of P. Subpanels as in ***Figure 2***. F) Summary of the effect of reducing connection density on the global SO frequency and amplitude as well as the standard deviation of the onset/offset delays (i.e. the width of the onset/offset histograms in d.5 / e.5)

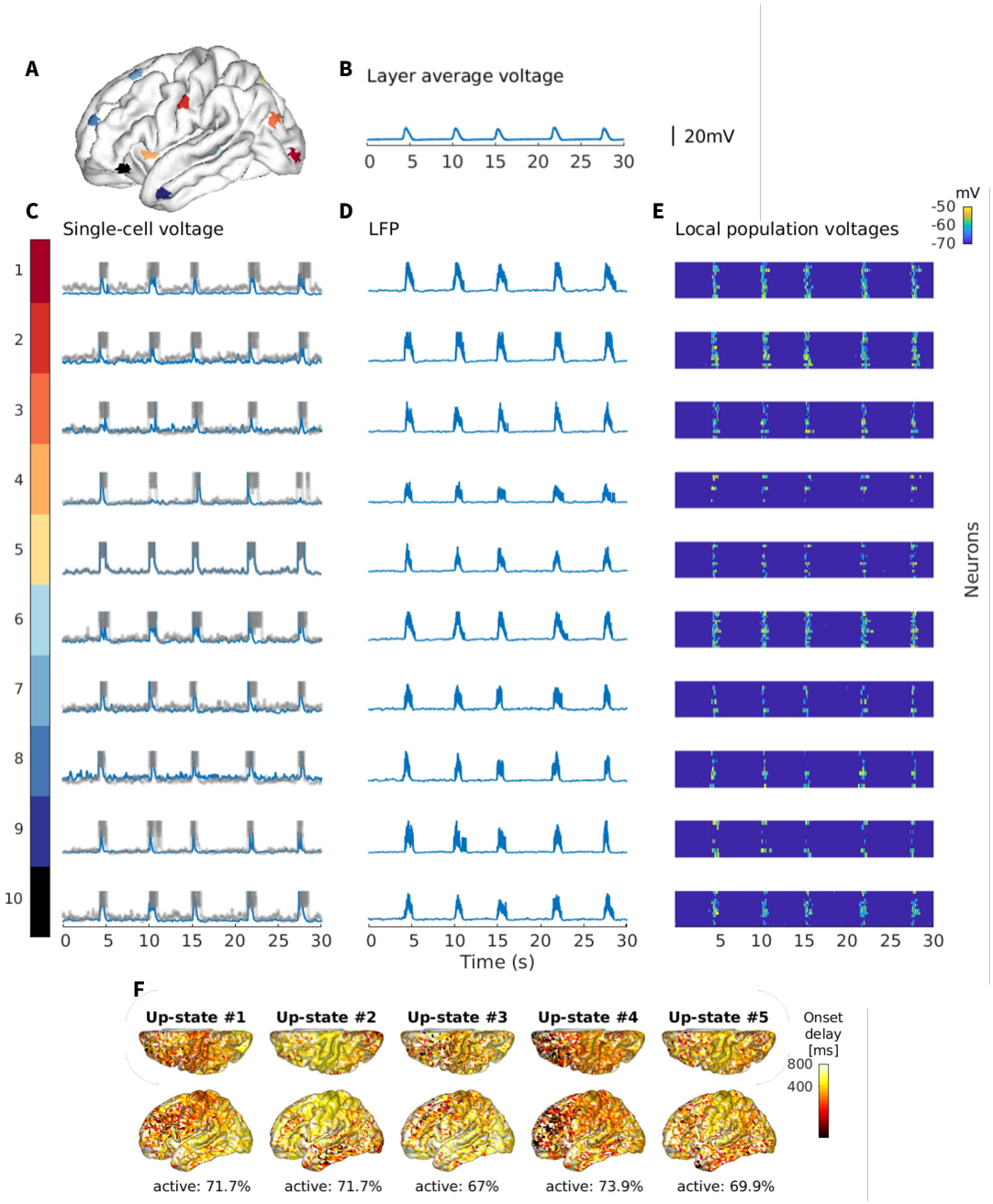

Figure 4. Local activity for $P = 0.1$, with 90% connections removed. A) Ten cortical areas with a 5mm radius, that were used to calculate local dynamics. B) Average membrane voltage of layer II neurons, as in ***Figure 3***e.2. C-E) For each region in (A), subpanels show: (C) the single-cell voltage for two neurons in the area , (D) the local field potential (LFP) for the 5mm area, and (E) heatmap of individual voltages of all neurons in the area. Up states are largely synchronized across all 5 regions. F) Latency map for each upstate in the $P = 0.1$ simulation. Even with very sparse connectivity, Up states spread to the whole cortex. Participation was reduced uniformly to about 70% compare to nearly 100% participation when all connections are present (compare to ***Figure 2***D)

connections (Connection Density). The network with a maximum connection radius of 5 mm (***Figure 5***D) showed no reduction in the frequency of the slow waves, but both the onsets and offsets of the slow waves revealed dramatic reduction in synchrony. Additionally, there was a substantial drop in slow wave propagation speed, while changes in connection density had minimal effect on speed (compare ***Figure 5***F and ***Figure 3***F). Despite all this, characteristic properties of global slow waves (high spread and high participation) found in baseline model were maintained.

However, reducing radius below 5mm (i.e., not including 2nd degree neighbors) caused a dramatic drop in global oscillation amplitude, akin to a phase transition from global to local oscillations. With a connection radius of 2.5 mm (***Figure 5***E), including only first order neighbors of each cell, global slow waves were largely lost in favor of local slow waves in small regions of the cortex (***Figure 6***, low spread, high participation). Note that this radius retains only 3.7% of connections; a spatially uniform drop to this fraction of connections ablated slow waves entirely. These local slow waves were generated in multiple initiation sites simultaneously, and occasionally showed regional propagation but never travelled across the full hemisphere (***Figure 6***F). This resulted in reduced global SO amplitude as long-range synchronicity between locally oscillating neural populations was impaired (***Figure 6***C-D). While a large fraction of the cortex was not participating in SO, the active regions were consistent across Up states. A connectivity analysis revealed that these regions correspond to the network areas with the highest node degree (see Supplementary ***Figure S4***). The same regions exhibited local slow waves for different simulations with the same connectivity parameters but different random seeds for network generation. This means that the active, i.e., generating local SO, areas are not random, but instead emerge from the underlying structure imposed by the dMRI connectivity data.

On the contrary, setting a minimum (rather than maximum) radius of up to 10 mm resulted in global slow waves that retained synchrony (not shown). In contrast to previous simulations, the initiation zones were here seen to resemble the edges of a circle and spread out, with silence in the epicenter: the lack of local connections made slow waves that "skip over" the most local regions to the initiation zone. An extreme case of 100 mm minimum radius (80% of connections removed) resulted in no defined initiation zone, but rather synchronized slow waves with diffuse initiation across the cortex.

As a whole, this analysis revealed that long range connections (longer than 5 mm) are essential for whole brain synchrony of the slow waves, but having only local connections (less than 5 mm) is still sufficient to make slow waves propagating over entire cortex (as long as remaining connections strength is scaled up to maintain total synaptic input per cell constant). Even with only first order neighbors, the network still maintained slow wave initiation, synchrony, and participation with local propagation.

Connection Delay

The model implements synaptic delays scaled by geodesic distance between neurons with a maximum delay of 40 ms. The majority of delays fall under 2 ms. To test the effects of delay times, we changed the delays in two ways (***Figure 7***): 1) by changing the maximum delay and scaling all others proportionally, and 2) by setting one uniform delay to all connections.

Setting the maximum delay to be smaller (all the way down to 0.1 ms) had little to no effect on slow wave amplitude, frequency, or synchronicity. Setting the maximum delay to be larger also had minimal effect on network activity until biologically implausible delays were implemented (≥1 second). Even at this extreme the network retained strong global slow waves, albeit with slightly lower amplitude, longer frequency, and de-synchronized onsets and offsets. Setting a uniform delay of 10 ms (where most delayes were previously under 2 ms) further left the network behavior largely unchanged. Only when the uniform delay was increased to 30 ms did we observe a loss of amplitude and synchrony (***Figure 7***). Since the delay times here shown to have an effect on network behavior are clearly beyond the range of biological plausibility, these results indicate that synaptic delays are not the primary determinant of slow wave spatio-temporal properties.

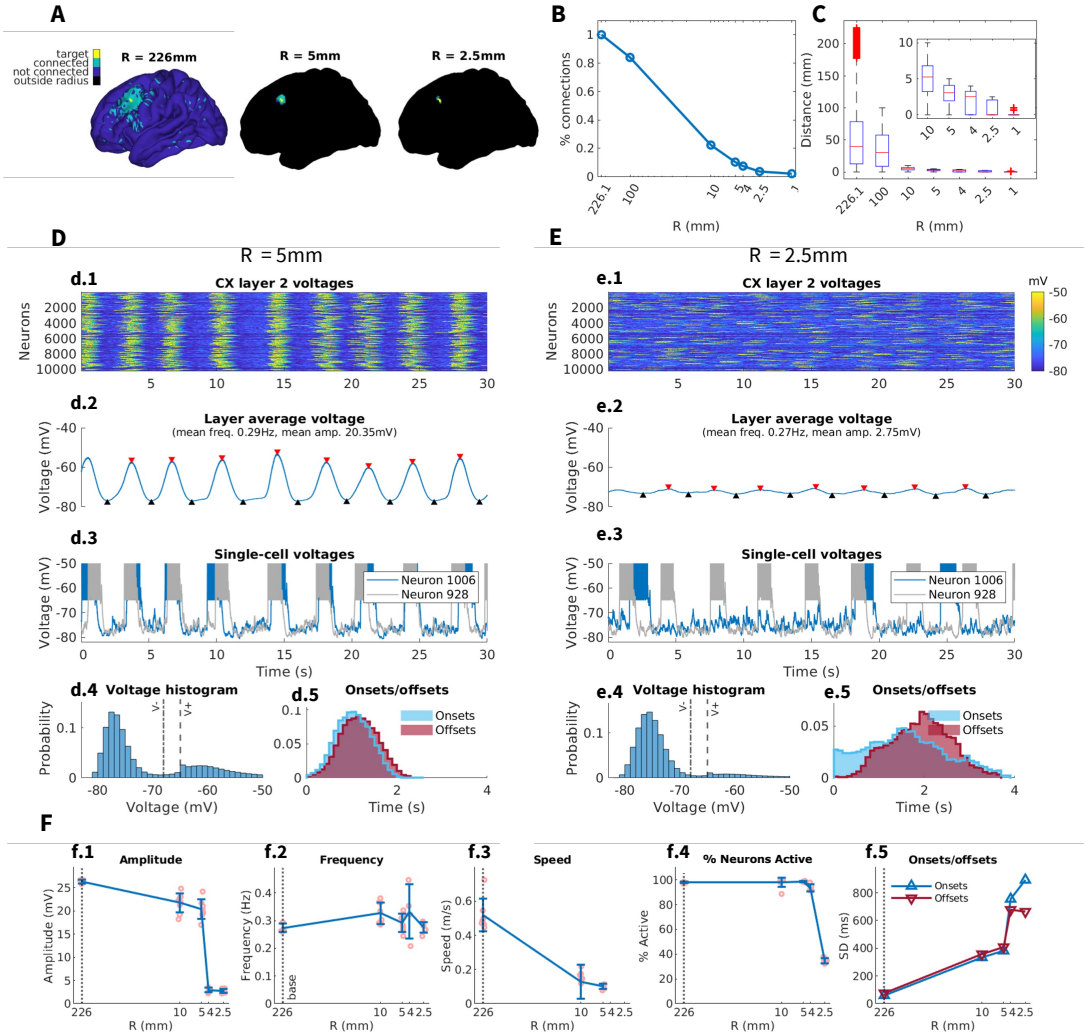

Figure 5. Effect of connection range on SO dynamics. A) Example target column (*yellow*) with all its connected columns (*green*). The *blue* area indicates the connection range for the corresponding radius R. No connections are made in the *black* region outside the radius. $R = 226mm$ encompasses all the original dMRI-derived connections. B) Percent of the original number of connections preserved for different values of R. C) Distance distribution for different values of R, with *inset* zooming into radii below 10mm. R imposes a maximum connection length and truncates the distance distribution accordingly. Red horizontal lines indicate medians, bottom and top box edges indicate the 25th and 75th percentiles, respectively, whiskers extend to the most extreme data points not considered outliers, and outliers are plotted individually using the '+' marker symbol. D-E) SO analysis for $R = 5mm$ and $R = 2.5mm$. Subpanels as in ***Figure 2***. F) Summary of the effect of reducing connection density on the global SO frequency and amplitude as well as the standard deviation of the onset/offset delays (i.e. the width of the onset/offset histograms in d.5 / e.5)

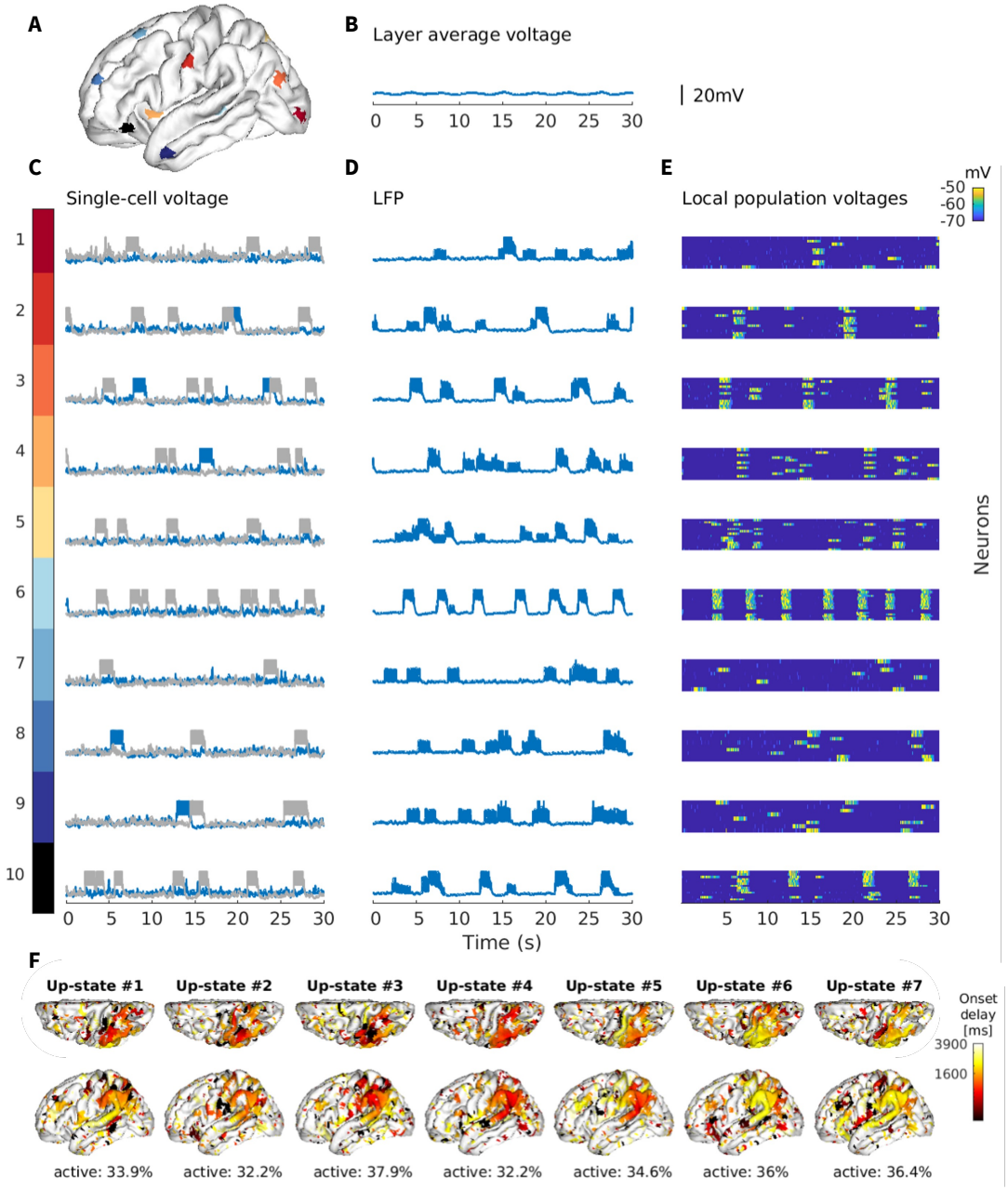

Figure 6. Local SO for small connection radius ($R = 2.5$mm). A) Ten cortical areas with a 5mm radius, that were used to calculate local dynamics. B) Average membrane voltage of layer II neurons, as in ***Figure 5***e.2. C-E) For each region in (A), subpanels show (C) the single-cell voltage for two neurons in the area, (D) the local field potential (LFP) for the 5mm area, and (E) heatmap of individual voltages of all neurons in the area. Note that even within these very small regions, there are still subgroups of independently synchronized neurons. F) Latency map, calculated as the onset delay of each neuron with respect to the earliest onset, for each upstate identified in ***Figure 5***e.2. Note that even the most global of slow waves has very low participation, around 35%, and can be seen to consist of many extremely small initiation sites that generally do not spread.

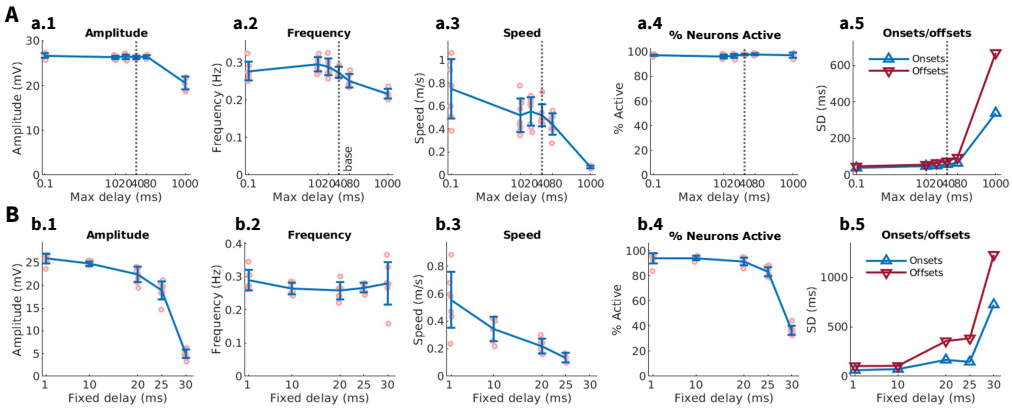

Figure 7. Effect of Synaptic Delay, either via setting a uniform delay (A) or scaling the max delay (B) on SO dynamics. (A & B) Summary plots of frequency, amplitude, and onset / offset spread. Decreasing the max scaled delay to 0.1 ms (from 40 ms) has no effect, while increasing the max scaled delay up to 1 second shows only minor changes in frequency & amplitude but notably increased onset/offfset synchrony. Low uniform delays similarly showed no effect, with loss of amplitude and synchrony only seen at 30 ms (most delays were previously under 2 ms).

Connection Strength

To probe the effects of absolute connection strength on the network activity, we varied the base connection strength between all cortical pyramidal neurons (***Figure 8***A, C). In contrast to experiments with changing connectivity density or radius, this changed the total synaptic input per cell. Weight reductions or increments by a factor of 4 or more caused the slow oscillations to be barely detectable or undetectable (note the low amplitude at the extremes of ***Figure 8***c.1). This was a result of low activity in the case of weights reduction, and of sustained Up state (Down state absence) in the case of weights increase. In general, within the detectable range, global SO amplitude, frequency, participation, and synchrony increased with synaptic strength (***Figure 8***C). Note that the model revealed an overall robustness to weight variation: the slow-wave propagation was minimally altered by strength increases or decreases by a factor of 2.

To further investigate the role of long range connectivity, we next performed 5x synaptic weight reductions on only "long-range connections" (i.e., connections over a defined minimum radius), and we varied the radius threshold from 2.5 mm to 50 mm (***Figure 8***B, D). Again, we did not scale the total synaptic input per cell, so these alternations affected balance of excitation and inhibition in the network. This experiment can be interpreted to model the phenomenon of stronger synaptic inputs nearest to the cell body (***Hawkins and Ahmad, 2016***; ***London and Segev, 2001***). We found that the global slow waves are lost when connections over 5mm are weakened (***Figure 8***d.1), however the local oscillatory activity, that does not spread through the entire cortex, can still be observed. This result also validates our earlier finding that the radius of 5 mm, which includs 2nd degree neighbors, is a critical inflection point in the network dynamics.

When we used a slightly higher threshold for long-range weight reduction, 10mm (***Figure 8***B, ***Figure 9***), the model displayed a number of clearly identifiable local slow waves originating and reliably traveling around the hemisphere in different directions (***Figure 9***F). Regularly, these local slow waves would coincide to produce a low-amplitude global slow wave in the LFP (see ***Figure 8***b.2, where red downward triangles mark the four detectable global Upstates analyzed in ***Figure 9***F). In this experiment, the local populations of neurons could synchronize but the gloabl synchrony was lost (***Figure 9***E). With reduced spread and high participation, this behavior resembles the results from simulations with exclusively local connectivity (see Connection Range), but stems from the more biologically reasonable assumption of weaker (rather than nonexistent) long range connectivity. Indeed, the propagation pattern in ***Figure 9*** is similar to the proposed pattern of biological

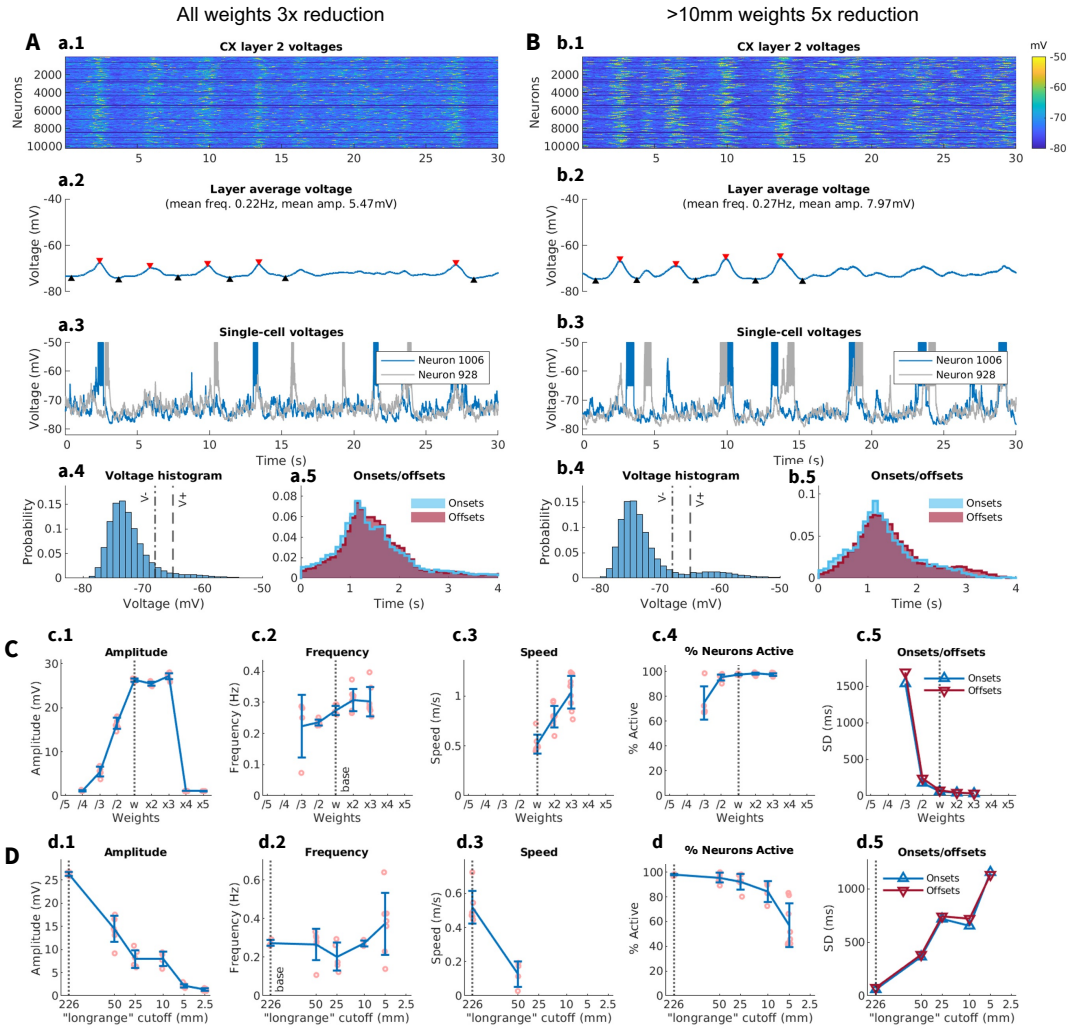

Figure 8. Effect of cortical excitatory synaptic strength on the network dynamics. A) Reduction of all cortical connections by 3x. B) Reduction of only connections longer than 10 mm by 5x. All subpanels as in ***Figure 2***. C) Summary of changes in frequency, amplitude, speed, participation, and onset/offset distribution spread when all connections are reduced as shown in (A). Increasing all weights shows little effect while decreasing all weights shows decreased amplitude & participation, with increases in onset/offset distributions (decreases in synchrony). The frequency of slow waves also becomes more variable. Note, Increasing all weights 5x results in the ablation of slow waves due to constant upstate, i.e., SO characteristics cannot be meaningfully quantified. D) Summary of changes in SO characteristics when only long range connections are reduced as shown in (B). Across all plots, 5 mm is seen to be an inflection point (or "elbow") where network activity changes.

Type II local slow waves as suggested by (***Siclari et al., 2014***; ***Nir et al., 2011***; ***Bernardi et al., 2018***; ***Funk et al., 2016***; ***Vyazovskiy et al., 2007***, ***2011***; ***Riedner et al., 2007***).

Discussion

Brain states are divided into wake, non-rapid eye movement (NREM), and REM sleep based on signatures in electroencephalogram (EEG) or local field potentials (LFPs). Deep NREM sleep is also called slow-wave sleep (SWS). It is characterized by the presence of slow waves (SWs) that might be accompanied with spindles. SWs are alternations of positive/negative EEG/LFP waves, also called slow oscillation (SO) (***Iber et al., 2007***). During depth positive waves cortical neurons are hyperpolarized (Down state), and during depth negative waves, they are depolarized (Up state) and fire action potentials (***Chauvette et al., 2010***; ***Steriade et al., 2001***; ***Timofeev et al., 2000b***, ***2001***). Sleep slow-waves have been actively studies in variety of species from rodents to humans. While local circuit mechanisms of SO generation have been sufficiently identified, the factors that define large-scale spatio-temporal SWS dynamics largely remain unknown. Here we present a whole-brain thalamocortical network model based on human dMRI connectivity data capable of generating awake state and sleep state with biologically realistic cortical slow waves. The model is applied to make specific predictions about effects of long- and short-range connectivity on spatio-temporal dynamics of slow-waves.

The sleep SO is hypothesized to be a cortical rhythm. This conclusion is based on three basic observations: (a) The slow oscillation survives extensive thalamic lesions (***Steriade et al., 1993a***), (b) the slow oscillation can be recorded in neocortical slices (***Sanchez-Vives and McCormick, 2000***) and isolated cortical slabs (***Timofeev et al., 2000a***), and (c) the slow oscillation is absent in the thalamus of decorticated cats (***Timofeev and Steriade, 1996***). Several mechanisms have been proposed to explain sleep SOs. The one, applied in our model here, depends on spontaneous miniature postsynaptic potentials (mPSPs) caused by the action potential-independent release of transmitter vesicles and regulated at the level of single synapses (***Timofeev et al., 2000a***; ***Bazhenov et al., 2002***). Occasional summation of the miniature EPSPs during the hyperpolarized (Down state) phase of SO activates the persistent sodium current and depolarizes the membrane of some cortical pyramidal cells sufficiently for spike generation. This triggers the spead of activity and active phase of SO, which is then maintained by synaptic activities and the persistent sodium current. Short-term synaptic depression and the activation of Ca^{2+}-dependent K^+ current terminate the active state (***Timofeev et al., 2000a***; ***Bazhenov et al., 2002***). While thalamus was not necessary to maintain SO in this model, it was later found, using a combination of in vivo electrophysiology and modeling, that the normal pattern of the neocortical SO requires thalamic inputs to synchronize activity across large cortical areas (***Lemieux et al., 2014***). Inactivation specific thalamic regions led to the loss of synchrony and periodicity of SO in the target cortical cell populations.

In other studies, it was proposed that transitions from Down to the Up state of SO may be initiated by spontaneous spike discharges in a random group of neurons (***Compte et al., 2003***), progressive activation of persistent Na^+ current (***Hill and Tononi, 2005***) or recurrent connections between cortical neurons within a given layer (presumably Layer V) (***Destexhe, 2009***). Once started, Up states are maintained by strong recurrent excitation, and the transitions to the Down state are due to a slow Na^+-dependent K^+ and/or depolarization-activated K^+ currents. In vitro studies suggest that a group of neurons, which initiate active periods could be either layer V IB neurons (***Sanchez-Vives and McCormick, 2000***) or spatially structured neuronal ensembles (***Cossart et al., 2003***). Bursting in thalamocortical neurons was proposed as an alternative mechanism triggering Down to Up state transitions in cortical populations (***Crunelli and Hughes, 2010***). While the above studies assume that there is an active process that leads to the Down to Up state transition, a recent study (***Levenstein et al., 2019***) proposed a model of slow oscillation generation where a stable active state is interrupted by transient inactive states. The model predicted how the level of drive and the relative strength of recurrent excitation and adaptation may create a spectrum of dynamical regimes with transitions between Up and Down states.

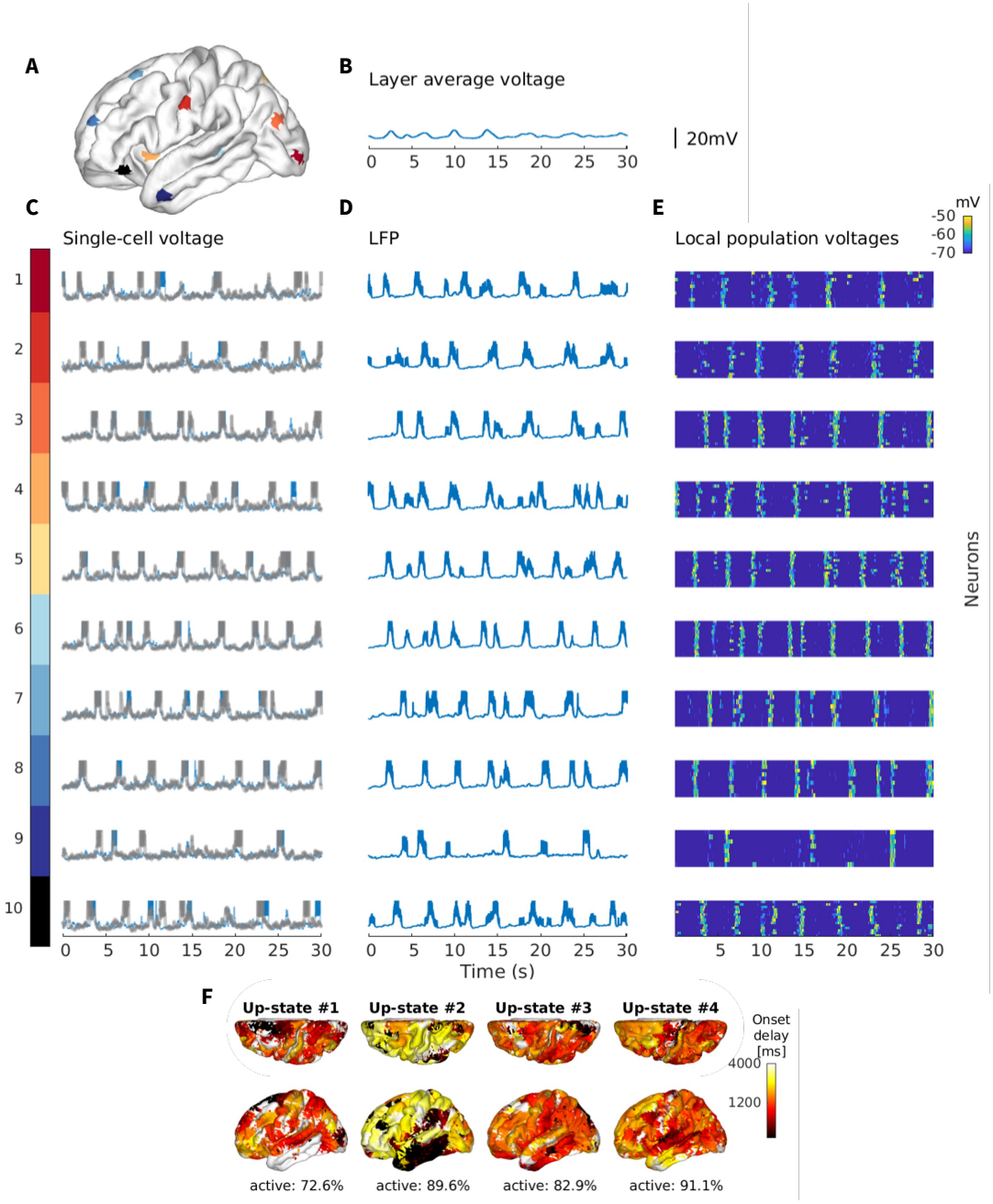

Figure 9. Local (type II) Slow Waves. A) Ten cortical areas with a 5mm radius, that were used to calculate local dynamics. B) Average membrane voltage of layer II neurons. C-E) For each region in (A), subpanels show (C) the single-cell voltage for two neurons in the area, (D) the local field potential (LFP) for the 5mm area, and (E) heatmap of individual voltages of all neurons in the area. This demonstrates that while there is some alignment, up states are not strongly global. F) Latency map, calculated as the onset delay of each neuron with respect to the earliest onset, for each upstate. Note, that while some Up states are global, others are comprised of several independent but coinciding local events.

	Density ⇓	Radius ⇓	Delay ⇑	Strength ⇓	Long Range Strength ⇓
Frequency	⇓	-	↓	⇓	-
Amplitude	⇓	⇓	↓	⇓	⇓
Speed	-	⇓	-	-	⇓
Synchrony	⇓	⇓	↓	⇓	⇓
Participation	⇓	-	-	-	-
Spread	Global	Local	Global	Global	Local

Table 1. Summary of results for each network manipulation. Decreasing connection density resulted in decreased slow wave frequency, amplitude, synchrony, and spread, but slow waves remained global. Decreasing connection radius resulted in decreased slow wave amplitude, speed, participation, and spread. Increasing delayed resulted in effects are seen only for manipulations far past biological plausibility, as indicated with a single down arrow for frequency, amplitude, and participation. Decreases in synaptic strength caused reduced amplitude, synchrony, frequency and participation. Finally, decreasing the strength of only long range connections resulted in traveling local slow waves with decreased amplitude, speed, and synchrony.

While many of these mechanisms have been explored in small local circuit models, only a few very recent studies (***Cakan et al., 2022***; ***Goldman et al., 2023***) have proposed simulating realistic long-range cortical connectivity to test its effect on the spatio-temporal properties of SO. While taking an important step in the direction of utilizing global brain connectivity data to study SWS, these models applied a mean-field neural-mass representation of cortical regions, which limits their applicability to studying how the interaction of local (within a few millimeters) and long-range connectivity affects spatio-temporal SWS dynamics.

In our approach, we developed a model based on spiking excitatory and inhibitory neurons in thalamus and cortex, organized in 6 cortical layers and thalamic core and matrix subsystems, with connectivity based on Human Connectome Project (HCP) diffusion-MRI (dMRI) tractography- based connection probabilities and HCP-derived degree of bulk myelination (***Rosen and Halgren, 2021***). To test contribution of specific elements of connectivity to SO properties, we then systematically modified selected elements of the network connectivity: connection density and radius, synaptic delays and strength.

We found that the network dynamics was robust to even significant decrease in connection density, but extreme reduction of the total number of connections by 90% resulted in less synchronous and less frequent slow waves that propagated sparsely through all the cortical regions and involved only a small fraction of all cortical neurons. We label this regime as high *spread* (defined as how far the slow wave travels across the cortex) and low *participation* (defined as the percent of neurons that participates in the slow wave within the area of spread). Equally severe restricting the connection radius, however, showed a loss of *synchrony* of SO Up-to-Down and Down-to-Up transitions but no reduction in SO frequency, spread, or participation. When only local (first order neighbor) connections were retained, slow waves reached high participation within local areas but lost the ability to spread across the entire cortex. As a whole, these results support the vital role of long range connections in network-wide synchrony, even if those connections are severely sparse.

Within a physiological range, changes in synaptic delays showed very little effect on SO dynamics. Similarly, increasing synaptic strength across all cortical excitatory connections had little effect on slow waves, besides slightly increasing the speed of propagation, up to the point when Down states were ablated. Decreasing strength, however, resulted in large drops in slow wave amplitude and participation, paired with more variability in the frequency and Up states onset/offset distribution. Eventually, with a 5 fold reduction, slow waves were entirely ablated.

When only connections longer than 5 mm were reduced in strength, it resulted in the ablation of global slow waves in favor of highly local oscillatory activity. Reducing strength of connections longer than 10 mm led to a combination of seemingly global and coinciding local slow waves partially propagating throughout the network, similar to results reported in vivo (***Nir et al., 2011***; ***Funk***

et al., 2016). These findings suggest existence of a minimal length of long-range connections (5-10 mm) necessary for global slow-waves to persist. Interestingly, *Riedner et al.* (*2007*) and *Vyazovskiy et al.* (*2007*) have reported that occurrence of multi-peak slow waves, where each peak has a different location of origin, increases over the course of sleep, which was proposed to result from a gradual net decrease in the strength of cortico-cortical connections (*Vyazovskiy et al.* (*2009*)). *Siclari et al.* (*2014*) and *Bernardi et al.* (*2018*) reported two types of slow waves: Type I - global and occurring earlier in sleep, and Type II - local slow waves found later in sleep. Our model revealed both of these types of slow waves and predicted the role of sleep homeostasis, manifested in progressive reduction of cortico-cortical connection strength, in explaining the data.

In our model, the neurons generally spend more time in Down than Up states, and slow-wave travels as a wave of activity, rather than silence. This is likley a result of still very low density on neurons (6 per column) in our model. Although our model design achieves high computational efficiency considering the size and complexity of the network, the number of model parameters and simulation time do not currently allow a systematic fitting of the model output to electrophysiological brain signals, as it has been done with smaller computational models (*Cakan et al., 2022*). Nevertheless, the use of realistic parameters for individual neuron dynamics in wake and sleep stages (*Bazhenov et al., 2002*; *Krishnan et al., 2016*) as well as experimentally grounded cortical connectivity (*Rosen and Halgren, 2021*) allowed us to reproduce the essential characteristics of activity in awake and SWS brain states. Our model allows to reproduce and to study biologically realistic whole-brain sleep dynamics, and still provides access to the cellular level resolution to study contribution of individual cell and local circuit properties.

In summary, we present a whole-brain thalamocortical network model constrained by realistic local and long range connectivity based on human dMRI data and implementing effects of neuromodulators to account for sleep-wake transitions. The model displays both a biologically realistic awake state with characteristic random neuron firing as well as Type I and Type II slow wave sleep dynamics. Importantly, it provides both the scale and the level of details required to investigate how large-scale sleep dynamics arise from cellular and circuit level activity. In general, we found slow waves to be highly robust to network decimation. This is in line with previous studies showing slow wave resilience to external perturbations (*Steriade et al., 1993b*), as well as with the intuition that a brain function as crucial as sleep would necessarily need to be robust. Nevertheless, loss of efficient long range connectivity led to significant alternations of the slow-wave patterns found in intact model, specifically transition from global slow waves to local sleep dynamics, suggesting possible mechanisms of sleep changes in aging or Alzheimer's disease. We propose this model can be further used to investigate sleep disorders and dysfunctions - both how they arise, and how they may be remedied.

Methods

Model Structure

Our whole brain computational model has realistic local and long-range cortical connectivity. The model has 10,242 cortical columns uniformly positioned across the surface of one hemisphere. Each column has 6 cortical layers of computationally efficient map-based neurons (*Komarov et al., 2018*), both excitatory (PY) and inhibitory (IN). Connections within the column follow those described in the canonical cortical circuit (*Figure 1* A). Additionally, connections within 0.1 mm are strengthened by a factor of 5 to mimic in-vivo increased strength of proximal synapses (*London and Segev, 2001*; *Hawkins and Ahmad, 2016*). Inhibition is local: IN cells project only to PY cells in the same layer, with connections only in their own column, 1st and 2nd degree neighbors. The strength of inhibitory synapses is 2 times larger within the local column than outside. Finally, miniature postsynaptic potentials on intracortical AMPA synapses are modeled as a Poisson process (as in *Krishnan et al.* (*2018*)).

Thalamocortical (TC) and reticular (RE) neurons are modeled using Hodgkin-Huxley dynamics

(***Hodgkin and Huxley, 1952***), with 2 subtypes of each to represent matrix and core neurons. The matrix TC neurons have a 45 mm (& 80 mm) fanout radii to cortical excitatory (& inhibitory) neurons while core TC neurons have 12 mm & 13 mm radii, respectively. Within-thalamic connections have 11 mm radii. There are 642 neurons of each of these 4 types (thalamic matrix, thalamic core, reticular matrix, reticular core).

Hierarchically Guided Laminar Connectivity

Long-range connectivity in the model is primarily based on the cortical parcellation into 180 areas per hemisphere proposed by the Human Connectome Project (HCP)-PPM1.0 atlas (***Van Essen et al., 2013***; ***Glasser et al., 2016***). Each parcel was assigned a hierarchical index inversely proportional to its estimated bulk myelination (***Glasser and Essen, 2011***; ***Burt et al., 2018***). Excitatory cortical connections (PY-PY) were then split into 6 classes according to the pre- and post-synaptic hierarchical index: within the local column, within the local parcel (or between contralateral homologs), strongly or weakly feedforward (from lower to higher hierarchical index), and strongly or weakly feedback (from higher to lower hierarchical index). Based on previous connectivity reports (***Markov et al., 2013***; ***Rockland, 2019***), synaptic weights for these connections were scaled by the factors shown in ***Figure 1*** D.

Diffusion MRI Guided Connection Probability

The connection probability was further scaled based on previous diffusion MRI (dMRI) connectivity studies (***Rosen and Halgren, 2021***). These observations reveal an exponential decay relationship between inter-parcel dMRI connectivity and fiber distance (length constant $\lambda = 23.4mm$, scaling parameter $\beta = 0.17$). In order to obtain a probability of connection at the scale of columns, intercolumnar geodesic distances were converted into estimated fiber distances. At the level of parcels, intrahemispheric dMRI streamline distances and their corresponding geodesic distances were found to be related to a first approximation by a linear rational function

$$F(x) = \frac{(p1 * x + p2)}{(x + q1)},$$

with $p1 = 295.6, p2 = -2256$, and $q1 = 69.4$, where x denotes the geodesic distance. Columwise fiber distances were estimated by applying this function to intercolumnar geodesic distances. Thus, a distance-dependent probability of connection between columns was obtained by applying the dMRI exponential relation to columwise fiber distances (***Figure 1*** E). Moreover, the residual parcelwise dMRI connectivity (not distance related, obtained by regressing out the exponential trend) was added back to intercolumnar connections based on the columns' parcels. This distance-independent connectivity accounts for the functional specialization of each parcel. Lastly, conduction delays were set to be proportional to fiber tract distances, with the longest connection (~226mm) having an assigned delay of 40ms.

Modifying Network Structure

We here attempted to create the most biologically realistic model and connectivity possible. However, there is no ground truth to dictate the absolute strength of connection between two individual neurons. While rules exist in our architecture to modify relative strength based on biological connectivity, the base connection strength to be modified is a completely free (and incredibly important) parameter. We first set the base strength level to be high enough to generate Type I slow waves which quickly synchronize across the entire brain. This makes slow wave property analysis more straightforward and less prone to spatial bias when modifying further network parameters, as is the goal of this paper. Hence, we use this global Type I slow wave model for all subsequent analysis aside from analyzing the effect of connection strength itself.

In the case of modulating connection density and range, the synaptic strengths were scaled up proportionally to the loss of connections to retain sufficient activity levels in the network. This

allowed us to isolate the effects of patterns of connection apart from changes in total synaptic input. The ablation of connections in these trials was accomplished by setting synaptic connection strengths to 0, removing all functional connectivity.

Onset/offset Detection and Latency

In order to characterize how SO spread through the cortex, we identified the points in time when each neuron transitions from downstate to upstate (onset) and viceversa (offset). Our upstate detection algorithm follows ***Komarov et al.*** (***2018***), based on ***Volgushev et al.*** (***2011***): we set two thresholds, $V^+ = -65$mV and $V^- = -68$mV (see dashed vertical lines in voltage histogram of ***Figure 2*** B), and label any activity above V^+ as an upstate and any activity below V^- as a downstate. This initial detection is further refined by merging any two upstates (or downstates) that are less than 100ms apart, and then removing any remaining upstate (or downstate) that lasts less than 100ms, in a similar approach to ***Volgushev et al.*** (***2011***).

To identify onsets and offsets for a particular global upstate, we considered the time window between consecutive minima of the average voltage signal around that upstate (e.g. see black upward triangles in average voltage signal of ***Figure 2*** B). For each neuron, we found the first time (if any) in this window when it reached an upstate (onset), and then the first time after the onset when it reached a downstate (offset). The minimum onset was then subtracted from all onsets so that the earliest neuron would have an assigned time of 0 and all other would have positive delays, or *latencies*. Similarly, the earliest offset was subtracted from all offsets.

In order to evaluate the synchronicity of active and silent states, we constructed aggregated histograms of the onset and offset times across all upstates of each simulation. We used the standard deviation of the histograms as an measure for synchrony, with narrow histograms indicating highly synchronized global upstates.

Latency maps are shown in ***Figure 2*** F (also ***Figure 4*** F, ***Figure 6*** F and ***Figure 9*** F) for each global upstate, representing the delay for activation of each cell after the earliest onset in that upstate. The 3D representation of latencies allows for a visual identification of the source (or sources) of each global upstate, characterized by clusters of adjacent neurons with near-zero latencies.

Acknowledgments

1R01MH117155, 1R01NS109553, 1R01MH125557

References

Bazhenov M, Timofeev I, Steriade M, Sejnowski TJ. Cellular and Network Models for Intrathalamic Augmenting Responses During 10-Hz Stimulation. Journal of Neurophysiology. 1998 May; 79(5):2730–2748. https://journals.physiology.org/doi/full/10.1152/jn.1998.79.5.2730, doi: 10.1152/jn.1998.79.5.2730, publisher: American Physiological Society.

Bazhenov M, Timofeev I, Steriade M, Sejnowski TJ. Computational Models of Thalamocortical Augmenting Responses. Journal of Neuroscience. 1998 Aug; 18(16):6444–6465. https://www.jneurosci.org/content/18/16/6444, doi: 10.1523/JNEUROSCI.18-16-06444.1998, publisher: Society for Neuroscience Section: ARTICLE.

Bazhenov M, Timofeev I, Steriade M, Sejnowski TJ. Model of Thalamocortical Slow-Wave Sleep Oscillations and Transitions to Activated States. The Journal of Neuroscience. 2002 Oct; 22(19):8691–8704. https://www.jneurosci.org/lookup/doi/10.1523/JNEUROSCI.22-19-08691.2002, doi: 10.1523/JNEUROSCI.22-19-08691.2002.

Bernardi G, Siclari F, Handjaras G, Riedner BA, Tononi G. Local and Widespread Slow Waves in Stable NREM Sleep: Evidence for Distinct Regulation Mechanisms. Frontiers in Human Neuroscience. 2018; 12. https://www.frontiersin.org/articles/10.3389/fnhum.2018.00248.

Bonjean M, Baker T, Lemieux M, Timofeev I, Sejnowski T, Bazhenov M. Corticothalamic Feedback Controls Sleep Spindle Duration In Vivo. Journal of Neuroscience. 2011 Jun; 31(25):9124–9134. https://www.jneurosci.org/lookup/doi/10.1523/JNEUROSCI.0077-11.2011, doi: 10.1523/JNEUROSCI.0077-11.2011.

Bonjean M, Baker T, Bazhenov M, Cash S, Halgren E, Sejnowski T. Interactions between Core and Matrix Thalamocortical Projections in Human Sleep Spindle Synchronization. The Journal of Neuroscience. 2012 Apr; 32(15):5250–5263. https://www.jneurosci.org/lookup/doi/10.1523/JNEUROSCI.6141-11.2012, doi: 10.1523/JNEUROSCI.6141-11.2012.

Burt JB, Demirtaş M, Eckner WJ, Navejar NM, Ji JL, Martin WJ, Bernacchia A, Anticevic A, Murray JD. Hierarchy of transcriptomic specialization across human cortex captured by structural neuroimaging topography. Nature Neuroscience. 2018 Sep; 21(9):1251–1259. doi: 10.1038/s41593-018-0195-0.

Cakan C, Dimulescu C, Khakimova L, Obst D, Flöel A, Obermayer K. Spatiotemporal Patterns of Adaptation-Induced Slow Oscillations in a Whole-Brain Model of Slow-Wave Sleep. Frontiers in Computational Neuroscience. 2022; 15. https://www.frontiersin.org/articles/10.3389/fncom.2021.800101.

Campbell SS, Tobler I. Animal sleep: A review of sleep duration across phylogeny. Neuroscience & Biobehavioral Reviews. 1984 Sep; 8(3):269–300. https://linkinghub.elsevier.com/retrieve/pii/014976348490054X, doi: 10.1016/0149-7634(84)90054-X.

Chauvette S, Volgushev M, Timofeev I. Origin of Active States in Local Neocortical Networks during Slow Sleep Oscillation. Cerebral Cortex. 2010 Nov; 20(11):2660–2674. https://academic.oup.com/cercor/article-lookup/doi/10.1093/cercor/bhq009, doi: 10.1093/cercor/bhq009.

Compte A, Sanchez-Vives MV, McCormick DA, Wang XJ. Cellular and Network Mechanisms of Slow Oscillatory Activity (<1 Hz) and Wave Propagations in a Cortical Network Model. Journal of Neurophysiology. 2003 May; 89(5):2707–2725. https://www.physiology.org/doi/10.1152/jn.00845.2002, doi: 10.1152/jn.00845.2002.

Cossart R, Aronov D, Yuste R. Attractor dynamics of network UP states in the neocortex. Nature. 2003 May; 423(6937):283–288. https://www.nature.com/articles/nature01614, doi: 10.1038/nature01614, number: 6937 Publisher: Nature Publishing Group.

Crunelli V, Hughes SW. The slow (<1 Hz) rhythm of non-REM sleep: a dialogue between three cardinal oscillators. Nature Neuroscience. 2010 Jan; 13(1):9–17. https://www.nature.com/articles/nn.2445, doi: 10.1038/nn.2445, number: 1 Publisher: Nature Publishing Group.

Destexhe A. Self-sustained asynchronous irregular states and Up-Down states in thalamic, cortical and thalamocortical networks of nonlinear integrate-and-fire neurons. Journal of Computational Neuroscience. 2009 Dec; 27(3):493–506. doi: 10.1007/s10827-009-0164-4.

Destexhe A, Contreras D, Steriade M. Spatiotemporal Analysis of Local Field Potentials and Unit Discharges in Cat Cerebral Cortex during Natural Wake and Sleep States. The Journal of Neuroscience. 1999 Jun; 19(11):4595–4608. https://www.ncbi.nlm.nih.gov/pmc/articles/PMC6782626/, doi: 10.1523/JNEUROSCI.19-11-04595.1999.

Donoghue T, Haller M, Peterson EJ, Varma P, Sebastian P, Gao R, Noto T, Lara AH, Wallis JD, Knight RT, Shestyuk A, Voytek B. Parameterizing neural power spectra into periodic and aperiodic components. Nature Neuroscience. 2020 Dec; 23(12):1655–1665. https://www.nature.com/articles/s41593-020-00744-x, doi: 10.1038/s41593-020-00744-x, number: 12 Publisher: Nature Publishing Group.

Funk CM, Honjoh S, Rodriguez AV, Cirelli C, Tononi G. Local slow waves in superficial layers of primary cortical areas during REM sleep. Current biology : CB. 2016 Feb; 26(3):396–403. https://www.ncbi.nlm.nih.gov/pmc/articles/PMC4747819/, doi: 10.1016/j.cub.2015.11.062.

Glasser MF, Coalson TS, Robinson EC, Hacker CD, Harwell J, Yacoub E, Ugurbil K, Andersson J, Beckmann CF, Jenkinson M, Smith SM, Van Essen DC. A multi-modal parcellation of human cerebral cortex. Nature. 2016 Aug; 536(7615):171–178. https://www.nature.com/articles/nature18933, doi: 10.1038/nature18933.

Glasser MF, Essen DCV. Mapping Human Cortical Areas In Vivo Based on Myelin Content as Revealed by T1- and T2-Weighted MRI. Journal of Neuroscience. 2011 Aug; 31(32):11597–11616. https://www.jneurosci.org/content/31/32/11597, doi: 10.1523/JNEUROSCI.2180-11.2011, publisher: Society for Neuroscience Section: Articles.

Goldman JS, Kusch L, Aquilue D, Yalçınkaya BH, Depannemaecker D, Ancourt K, Nghiem TAE, Jirsa V, Destexhe A. A comprehensive neural simulation of slow-wave sleep and highly responsive wakefulness dynamics. Frontiers in Computational Neuroscience. 2023 Jan; 16:1058957. https://www.frontiersin.org/articles/10.3389/fncom.2022.1058957/full, doi: 10.3389/fncom.2022.1058957.

Hawkins J, Ahmad S. Why Neurons Have Thousands of Synapses, a Theory of Sequence Memory in Neocortex. Frontiers in Neural Circuits. 2016 Mar; 10:23. https://www.ncbi.nlm.nih.gov/pmc/articles/PMC4811948/, doi: 10.3389/fncir.2016.00023.

Hill S, Tononi G. Modeling Sleep and Wakefulness in the Thalamocortical System. Journal of Neurophysiology. 2005 Mar; 93(3):1671–1698. https://journals.physiology.org/doi/full/10.1152/jn.00915.2004, doi: 10.1152/jn.00915.2004, publisher: American Physiological Society.

Hodgkin AL, Huxley AF. A quantitative description of membrane current and its application to conduction and excitation in nerve. The Journal of Physiology. 1952 Aug; 117(4):500–544. https://www.ncbi.nlm.nih.gov/pmc/articles/PMC1392413/, doi: 10.1113/jphysiol.1952.sp004764, publisher: Wiley-Blackwell.

Iber C, Ancoli-Israel S, Chesson A, Quan S. Manual for the Scoring of Sleep and Associated Events: Rules, Terminology and Technical Specifications. American Academy of Sleep Medicine. 2007; 59.

Isomura Y, Sirota A, Özen S, Montgomery S, Mizuseki K, Henze DA, Buzsáki G. Integration and Segregation of Activity in Entorhinal-Hippocampal Subregions by Neocortical Slow Oscillations. Neuron. 2006 Dec; 52(5):871–882. https://linkinghub.elsevier.com/retrieve/pii/S0896627306008221, doi: 10.1016/j.neuron.2006.10.023.

Ji D, Wilson MA. Coordinated memory replay in the visual cortex and hippocampus during sleep. Nature Neuroscience. 2007 Jan; 10(1):100–107. https://www.nature.com/articles/nn1825, doi: 10.1038/nn1825.

Komarov M, Krishnan G, Chauvette S, Rulkov N, Timofeev I, Bazhenov M. New class of reduced computationally efficient neuronal models for large-scale simulations of brain dynamics. Journal of Computational Neuroscience. 2018 Feb; 44(1):1–24. http://link.springer.com/10.1007/s10827-017-0663-7, doi: 10.1007/s10827-017-0663-7.

Krishnan GP, Chauvette S, Shamie I, Soltani S, Timofeev I, Cash SS, Halgren E, Bazhenov M. Cellular and neurochemical basis of sleep stages in the thalamocortical network. eLife. 2016 Nov; 5:e18607. https://elifesciences.org/articles/18607, doi: 10.7554/eLife.18607.

Krishnan GP, Rosen BQ, Chen JY, Muller L, Sejnowski TJ, Cash SS, Halgren E, Bazhenov M. Thalamocortical and intracortical laminar connectivity determines sleep spindle properties. PLOS Computational Biology. 2018 Jun; 14(6):e1006171. https://journals.plos.org/ploscompbiol/article?id=10.1371/journal.pcbi.1006171, doi: 10.1371/journal.pcbi.1006171, publisher: Public Library of Science.

Lee SH, Dan Y. Neuromodulation of Brain States. Neuron. 2012 Oct; 76(1):209–222. https://linkinghub.elsevier.com/retrieve/pii/S0896627312008203, doi: 10.1016/j.neuron.2012.09.012.

Lemieux M, Chen JY, Lonjers P, Bazhenov M, Timofeev I. The Impact of Cortical Deafferentation on the Neocortical Slow Oscillation. The Journal of Neuroscience. 2014 Apr; 34(16):5689–5703. https://www.jneurosci.org/lookup/doi/10.1523/JNEUROSCI.1156-13.2014, doi: 10.1523/JNEUROSCI.1156-13.2014.

Leung LC, Mourrain P. Sleep: Short Sleepers Should Keep Count of Their Hypocretin Neurons. Current Biology. 2018 May; 28(9):R558–R560. https://linkinghub.elsevier.com/retrieve/pii/S0960982218303075, doi: 10.1016/j.cub.2018.03.006.

Levenstein D, Buzsáki G, Rinzel J. NREM sleep in the rodent neocortex and hippocampus reflects excitable dynamics. Nature Communications. 2019 Jun; 10(1):2478. https://www.nature.com/articles/s41467-019-10327-5, doi: 10.1038/s41467-019-10327-5.

London M, Segev I. Synaptic scaling in vitro and in vivo. Nature Neuroscience. 2001 Sep; 4(9):853–854. https://www.nature.com/articles/nn0901-853, doi: 10.1038/nn0901-853, number: 9 Publisher: Nature Publishing Group.

Markov NT, Ercsey-Ravasz M, Van Essen DC, Knoblauch K, Toroczkai Z, Kennedy H. Cortical high-density counterstream architectures. Science (New York, NY). 2013 Nov; 342(6158):1238406. doi: 10.1126/science.1238406.

Mölle M, Eschenko O, Gais S, Sara SJ, Born J. The influence of learning on sleep slow oscillations and associated spindles and ripples in humans and rats. European Journal of Neuroscience. 2009 Mar; 29(5):1071–1081. https://onlinelibrary.wiley.com/doi/10.1111/j.1460-9568.2009.06654.x, doi: 10.1111/j.1460-9568.2009.06654.x.

Nir Y, Staba RJ, Andrillon T, Vyazovskiy VV, Cirelli C, Fried I, Tononi G. Regional slow waves and spindles in human sleep. Neuron. 2011 Apr; 70(1):153–169. doi: 10.1016/j.neuron.2011.02.043.

Pfaff D, Ribeiro A, Matthews J, Kow L. *Concepts and Mechanisms of Generalized Central Nervous System Arousal*. Annals of the New York Academy of Sciences. 2008 May; 1129(1):11–25. https://nyaspubs.onlinelibrary.wiley.com/doi/10.1196/annals.1417.019, doi: 10.1196/annals.1417.019.

Rasch B, Büchel C, Gais S, Born J. Odor Cues During Slow-Wave Sleep Prompt Declarative Memory Consolidation. Science. 2007 Mar; 315(5817):1426–1429. https://www.science.org/doi/10.1126/science.1138581, doi: 10.1126/science.1138581.

Riedner BA, Vyazovskiy VV, Huber R, Massimini M, Esser S, Murphy M, Tononi G. Sleep Homeostasis and Cortical Synchronization: III. A High-Density EEG Study of Sleep Slow Waves in Humans. Sleep. 2007 Dec; 30(12):1643–1657. https://www.ncbi.nlm.nih.gov/pmc/articles/PMC2276133/.

Rockland KS. What do we know about laminar connectivity? NeuroImage. 2019 Aug; 197:772–784. doi: 10.1016/j.neuroimage.2017.07.032.

Rosanova M, Ulrich D. Pattern-Specific Associative Long-Term Potentiation Induced by a Sleep Spindle-Related Spike Train. The Journal of Neuroscience. 2005 Oct; 25(41):9398–9405. https://www.jneurosci.org/lookup/doi/10.1523/JNEUROSCI.2149-05.2005, doi: 10.1523/JNEUROSCI.2149-05.2005.

Rosen BQ, Halgren E. A Whole-Cortex Probabilistic Diffusion Tractography Connectome. eneuro. 2021 Jan; 8(1):ENEURO.0416–20.2020. https://www.eneuro.org/lookup/doi/10.1523/ENEURO.0416-20.2020, doi: 10.1523/ENEURO.0416-20.2020.

Sanchez-Vives MV, McCormick DA. Cellular and network mechanisms of rhythmic recurrent activity in neocortex. Nature Neuroscience. 2000 Oct; 3(10):1027–1034. https://www.nature.com/articles/nn1000_1027, doi: 10.1038/79848, number: 10 Publisher: Nature Publishing Group.

Shepherd GMG, Yamawaki N. Untangling the cortico-thalamo-cortical loop: cellular pieces of a knotty circuit puzzle. Nature Reviews Neuroscience. 2021 Jul; 22(7):389–406. https://www.nature.com/articles/s41583-021-00459-3, doi: 10.1038/s41583-021-00459-3.

Siclari F, Bernardi G, Riedner BA, LaRocque JJ, Benca RM, Tononi G. Two Distinct Synchronization Processes in the Transition to Sleep: A High-Density Electroencephalographic Study. Sleep. 2014 Oct; 37(10):1621–1637. https://www.ncbi.nlm.nih.gov/pmc/articles/PMC4173919/, doi: 10.5665/sleep.4070.

Steriade M. Impact of network activities on neuronal properties in corticothalamic systems. Journal of Neurophysiology. 2001 Jul; 86(1):1–39. doi: 10.1152/jn.2001.86.1.1.

Steriade M, Nunez A, Amzica F. Intracellular analysis of relations between the slow (< 1 Hz) neocortical oscillation and other sleep rhythms of the electroencephalogram. Journal of Neuroscience. 1993 Aug; 13(8):3266–3283. https://www.jneurosci.org/content/13/8/3266, doi: 10.1523/JNEUROSCI.13-08-03266.1993, publisher: Society for Neuroscience Section: Articles.

Steriade M, Timofeev I, Grenier F. Natural Waking and Sleep States: A View From Inside Neocortical Neurons. Journal of Neurophysiology. 2001 May; 85(5):1969–1985. https://journals.physiology.org/doi/full/10.1152/jn.2001.85.5.1969, doi: 10.1152/jn.2001.85.5.1969, publisher: American Physiological Society.

Steriade M, McCormick DA, Sejnowski TJ. Thalamocortical Oscillations in the Sleeping and Aroused Brain. Science. 1993 Oct; 262(5134):679–685. https://www.science.org/doi/10.1126/science.8235588, doi: 10.1126/science.8235588, publisher: American Association for the Advancement of Science.

Steriade MM, McCarley RW. Brainstem Control of Wakefulness and Sleep. Springer Science & Business Media; 2013. Google-Books-ID: X5juBwAAQBAJ.

Timofeev I, Grenier F, Bazhenov M, Sejnowski TJ, Steriade M. Origin of Slow Cortical Oscillations in Deafferented Cortical Slabs. Cerebral Cortex. 2000 Dec; 10(12):1185–1199. https://doi.org/10.1093/cercor/10.12.1185, doi: 10.1093/cercor/10.12.1185.

Timofeev I, Steriade M. Low-frequency rhythms in the thalamus of intact-cortex and decorticated cats. Journal of Neurophysiology. 1996 Dec; 76(6):4152–4168. https://journals.physiology.org/doi/abs/10.1152/jn.1996.76.6.4152, doi: 10.1152/jn.1996.76.6.4152, publisher: American Physiological Society.

Timofeev I, Grenier F, Steriade M. Impact of intrinsic properties and synaptic factors on the activity of neocortical networks in vivo. Journal of Physiology-Paris. 2000 Dec; 94(5):343–355. https://www.sciencedirect.com/science/article/pii/S0928425700010974, doi: 10.1016/S0928-4257(00)01097-4.

Timofeev I, Grenier F, Steriade M. Disfacilitation and active inhibition in the neocortex during the natural sleep-wake cycle: An intracellular study. Proceedings of the National Academy of Sciences. 2001 Feb; 98(4):1924–1929. https://www.pnas.org/doi/abs/10.1073/pnas.98.4.1924, doi: 10.1073/pnas.98.4.1924, publisher: Proceedings of the National Academy of Sciences.

Van Essen DC, Smith SM, Barch DM, Behrens TEJ, Yacoub E, Ugurbil K. The WU-Minn Human Connectome Project: An overview. NeuroImage. 2013 Oct; 80:62–79. https://www.sciencedirect.com/science/article/pii/S1053811913005351, doi: 10.1016/j.neuroimage.2013.05.041.

Volgushev M, Chauvette S, Timofeev I. Long-range correlation of the membrane potential in neocortical neurons during slow oscillation. In: *Progress in Brain Research*, vol. 193 Elsevier; 2011.p. 181–199. https://linkinghub.elsevier.com/retrieve/pii/B9780444538390000120, doi: 10.1016/B978-0-444-53839-0.00012-0.

Vyazovskiy VV, Olcese U, Hanlon EC, Nir Y, Cirelli C, Tononi G. Local sleep in awake rats. Nature. 2011 Apr; 472(7344):443–447. https://www.ncbi.nlm.nih.gov/pmc/articles/PMC3085007/, doi: 10.1038/nature10009.

Vyazovskiy VV, Olcese U, Lazimy YM, Faraguna U, Esser SK, Williams JC, Cirelli C, Tononi G. Cortical Firing and Sleep Homeostasis. Neuron. 2009 Sep; 63(6):865–878. https://linkinghub.elsevier.com/retrieve/pii/S0896627309006370, doi: 10.1016/j.neuron.2009.08.024.

Vyazovskiy VV, Riedner BA, Cirelli C, Tononi G. Sleep Homeostasis and Cortical Synchronization: II. A Local Field Potential Study of Sleep Slow Waves in the Rat. Sleep. 2007 Dec; 30(12):1631–1642. https://www.ncbi.nlm.nih.gov/pmc/articles/PMC2276140/.

Wierzynski CM, Lubenov EV, Gu M, Siapas AG. State-Dependent Spike-Timing Relationships between Hippocampal and Prefrontal Circuits during Sleep. Neuron. 2009 Feb; 61(4):587–596. https://linkinghub.elsevier.com/retrieve/pii/S0896627309000786, doi: 10.1016/j.neuron.2009.01.011.

Winkelman JW, Lecea LD. Sleep and neuropsychiatric illness. Neuropsychopharmacology. 2020 Jan; 45(1):1–2. https://www.nature.com/articles/s41386-019-0514-5, doi: 10.1038/s41386-019-0514-5.

Supplementary Information

Activity by Layer and Cell Type

Figure S1 shows the activity of all 6 modeled layers baseline SO simulation in ***Figure 2***. Activity is largely synchronized across layers.

Figure S2 shows the activity of modeled core and matrix thalamocortical (TC, TCa) and reticular (RE, REa) cells as well as inhibitory (IN) cells.

Graph Properties

Figure S3 and ***Figure S4*** show graph properties of the networks for the baseline slow wave simulation in ***Figure 2*** and for the restricted range $R = 2.5mm$ simulation in ***Figure 6***. For the full connectivity network, initiation zones (characterized by low mean onset delay) generally correspond to lower in-degree and out-degree regions. For the local connectivity network, active regions during Upstates in ***Figure 6***F correspond to regions with high in-degree and out-degree.

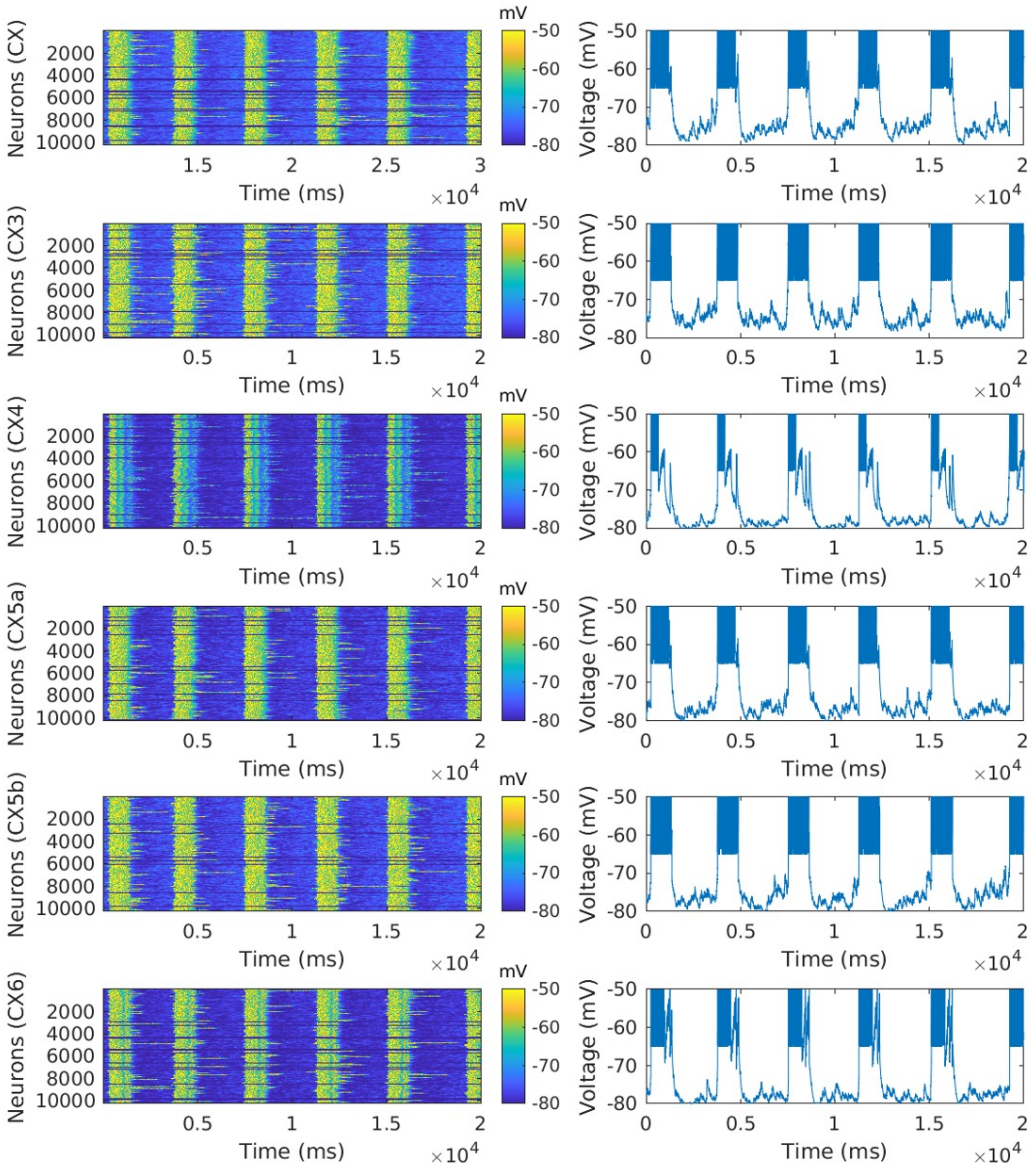

Figure S1. Neuronal activity in all 6 layers during the baseline SO simulation from ***Figure 2***

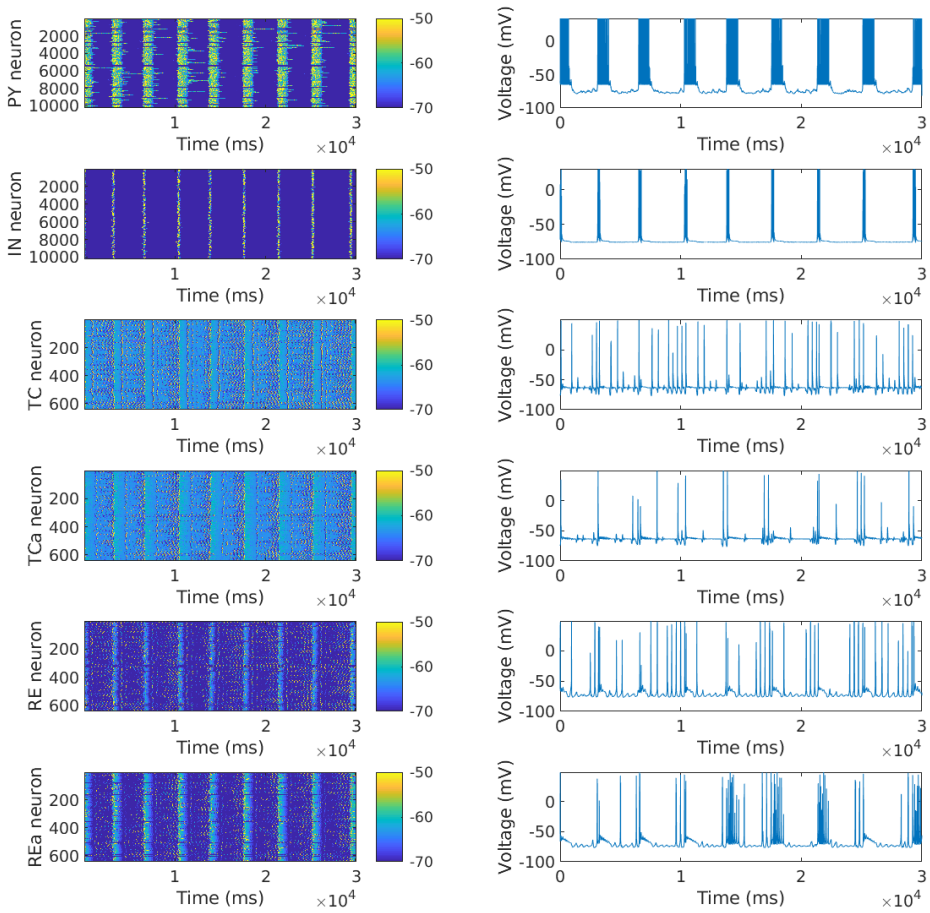

Figure S2. Activity of cortical inhibitory and thalamic RE and TC neurons.

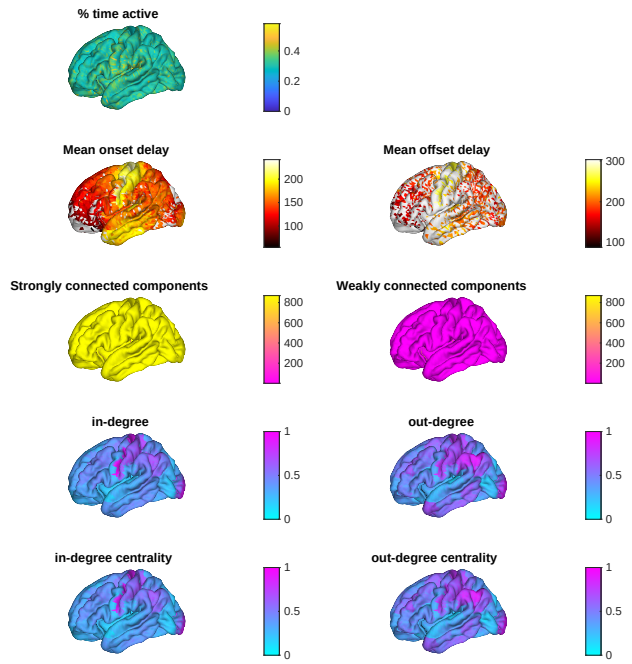

Figure S3. Graph properties for baseline network

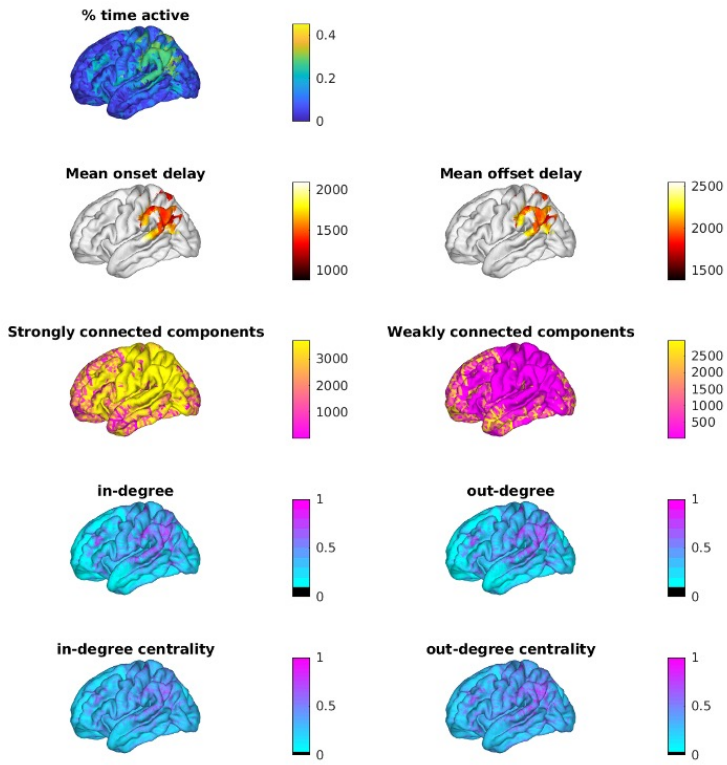

Figure S4. Graph properties for $R = 2.5$mm network